



HAL
open science

Adenylates regulate *Arabidopsis* plastidial thioredoxin activities through the binding of a CBS domain protein

Author names and affiliations

Kevin Baudry, Félix Barbut, Séverine Domenichini, Damien Guillaumot, Mai Pham Thy, Hélène Vanacker, Wojciech Majeran, Anja Krieger-Liszkay, Emmanuelle Issakidis-Bourguet, Claire Lurin

► To cite this version:

Kevin Baudry, Félix Barbut, Séverine Domenichini, Damien Guillaumot, Mai Pham Thy, et al.. Adenylates regulate *Arabidopsis* plastidial thioredoxin activities through the binding of a CBS domain protein Author names and affiliations. *Plant Physiology*, 2022, 189 (4), pp.2298-2314. hal-04304535

HAL Id: hal-04304535

<https://hal.science/hal-04304535v1>

Submitted on 24 Nov 2023

HAL is a multi-disciplinary open access archive for the deposit and dissemination of scientific research documents, whether they are published or not. The documents may come from teaching and research institutions in France or abroad, or from public or private research centers.

L'archive ouverte pluridisciplinaire **HAL**, est destinée au dépôt et à la diffusion de documents scientifiques de niveau recherche, publiés ou non, émanant des établissements d'enseignement et de recherche français ou étrangers, des laboratoires publics ou privés.

1 **Short title:** CBSX2 regulates Thioredoxins m in plastids

2 **Title:**

3 **Adenylates regulate Arabidopsis plastidial thioredoxin activities through the binding of**
4 **a CBS domain protein**

5 **Author names and affiliations:**

6 Kevin Baudry^{a,b}, Félix Barbut^{a,b}, Séverine Domenichini^{a,b,c}, Damien Guillaumot^{a,b}, Mai Pham
7 Thy^{a,b}, Hélène Vanacker^{a,b}, Wojciech Majeran^{a,b}, Anja Krieger-Liszkay^d, Emmanuelle
8 Issakidis-Bourguet^{a,b,*}, Claire Lurin^{a,b}

9 ^aUniversité Paris-Saclay, CNRS, INRAE, Univ Evry, Institute of Plant Sciences Paris-Saclay
10 (IPS2), 91190, Gif sur Yvette, France.

11 ^bUniversité Paris Cité, CNRS, INRAE, Institute of Plant Sciences Paris-Saclay (IPS2), 91190,
12 Gif sur Yvette, France.

13 ^cPresent address: Université Paris-Saclay, UMS IPSIT - US 31 INSERM - UMS 3679 CNRS

14 ^d Université Paris-Saclay, Institute for Integrative Biology of the Cell (I2BC), CEA, CNRS,
15 91198 Gif-sur-Yvette, France

16

17 ***Corresponding author:**

18 Emmanuelle Issakidis-Bourguet, IPS2, rue de Noetzlin, CS 80004, 91192 Gif sur Yvette
19 Cedex, tel: +33 1 69 15 33 37, email: [emmanuelle.issakidis-bourguet@universite-paris-](mailto:emmanuelle.issakidis-bourguet@universite-paris-saclay.fr)
20 [saclay.fr](mailto:emmanuelle.issakidis-bourguet@universite-paris-saclay.fr)

21 The author responsible for distribution of materials integral to the findings presented in this
22 article in accordance with the policy described in the Instructions for Authors
23 (<https://academic.oup.com/plphys/pages/General-Instructions>) is Emmanuelle Issakidis-
24 Bourguet.

25

26 **Author contributions:** C. L., E. I-B., W. M., H. V. and A. K-L. designed the research and
27 supervised the experiments; F. B., S. D., D. G. and M. P. T. performed experiments;. K. B.,
28 A. K-L. and E. I-B performed experiments and analyzed the data; K. B., C. L., A. K-L. and E.
29 I-B. wrote the manuscript.

30 **One-sentence summary:** A cystathionine- β -synthase protein inhibits thioredoxins m
31 activities towards NADP-malate dehydrogenase and 2-Cys peroxiredoxin in an adenylate-
32 dependent manner.
33 .

34 **ABSTRACT**

35 Cystathionine- β -synthase (CBS) domains are found in proteins of all living organisms and
36 have been proposed to play a role as energy sensors regulating protein activities through their
37 adenosyl ligand binding capacity. In plants, members of the CBSX protein family carry a
38 stand-alone pair of CBS domains. In *Arabidopsis thaliana*, CBSX1 and CBSX2
39 are targeted to plastids where they have been proposed to regulate thioredoxins (TRX). TRX
40 are ubiquitous cysteine thiol oxido-reductases involved in the redox-based regulation of
41 numerous enzymatic activities as well as in the regeneration of thiol-dependent peroxidases.
42 In *Arabidopsis*, 10 TRX isoforms have been identified in plastids and divided into five sub-
43 types. Here, we show that CBSX2 specifically inhibits the activities of m-type TRXs towards
44 two chloroplast TRX-related targets. By testing activation of NADP-malate dehydrogenase
45 and reduction of 2-Cys peroxiredoxin, we found that TRXm1/2 inhibition by CBSX2 was
46 alleviated in presence of AMP or ATP. We also evidenced, by pull-down assays, a direct
47 interaction of CBSX2 with reduced TRXm1 and m2 that was abolished in presence of
48 adenosyl ligands. In addition, we report that, in comparison to wild-type plants, the
49 *Arabidopsis* T-DNA double mutant *cbx1 cbx2* exhibits growth and chlorophyll
50 accumulation defects in cold conditions, suggesting a function of plastidial CBSX proteins in
51 plant stress adaptation. Altogether, our results show an energy sensing regulation of plastid
52 TRX m activities by CBSX, possibly allowing a feedback regulation of ATP homeostasis via
53 activation of cyclic electron flow in the chloroplast, to maintain a high energy level for
54 optimal growth.

55 INTRODUCTION

56 Plants depend on light for the generation of energy and reducing power in the forms of ATP
57 and NADPH produced in the chloroplasts and consumed in assimilatory processes.

58 The major role played by chloroplasts as the source and target of reduction–oxidation (redox)
59 regulation is now well established in plant cells (Baier and Dietz, 2005). Thioredoxins (TRX)
60 are key actors of the underlying complex redox regulatory network. TRX are small (~12kDa)
61 ubiquitous redox proteins found in all cellular compartments. Among the 20 isoforms encoded
62 by the Arabidopsis (*Arabidopsis thaliana*) genome, 10 are targeted to plastids and were sub-
63 divided in five groups (4 TRX m, 2 TRX f, 2 TRX y, 1 TRX x and 1 TRX z). In plastids,
64 TRX have numerous targets involved in various metabolic and stress response functions
65 (Gelhaye et al., 2005; Lemaire et al., 2007; Geigenberger et al., 2017). TRX can act either as
66 regulators of the activity of their targets by post-translational modification or as reducing
67 substrate for their target. TRX can activate their targets through direct disulfide bridge
68 reduction, as for example, plastidial NADPH-dependent malate dehydrogenase (NADP-
69 MDH). They can also provide reducing power to their targets as in case of the 2-cysteine
70 peroxiredoxin (2-Cys PRX) (Collin et al., 2003; Collin et al., 2004).

71 While the number of functions attributed to TRX in plastids is very large (Montrichard et al.,
72 2009), knowledge about their regulation is limited. In plastids, TRXs redox state mainly
73 depends on the balance between the “electron pressure” light-fueled by the photosynthetic
74 electron transport chain and the “oxidative pressure” of H₂O₂ (Vaseghi et al., 2018; Yoshida
75 and Hisabori, 2018). Data about additional factors directly regulating TRX redox state are
76 very scarce. For instance, TRX f was found glutathionylated and consequently losing its
77 capability to regulate its targets (Michelet et al., 2005). Yoo *et al.* (2011) suggested that
78 cystathionine-β-synthase proteins are ubiquitous regulators of TRXs in plastids to control
79 H₂O₂ levels and regulate lignin polymerization in the anther endothecium.

80 Cystathionine-β-synthase (CBS) domain (Pfam: PF00571) was identified in proteins from
81 bacteria, yeasts, animals and plants (Ignoul and Eggermont, 2005; Kushwaha et al., 2009;
82 Crozet et al., 2014; Shahbaaz et al., 2015). This small domain of approximately 60 amino
83 acids forms an antiparallel β-sheet flanked by helices on one side. It is generally found as a
84 tandem repeat forming a CBS pair or the so-called Bateman domain (Bateman, 1997) that
85 defines the CBS-Domain-Containing-Protein (CDCP) family (Ignoul and Eggermont, 2005).
86 Homodimers of CBS pairs are generally involved in the binding of regulatory adenosyl
87 ligands such as AMP, ATP or S-adenosylmethionine (Kemp, 2004; Ereño-Orbea et al., 2013).

88 Consequently, CBS domains were proposed to function as sensors of cell energy status (Scott
89 et al., 2004; Kushwaha et al., 2009). Associated to several different functional domains, in a
90 wide range of functionally different CDCP proteins, CBS domains act generally as regulatory
91 domains of protein activity through adenosyl ligand binding (Hardie and Hawley, 2001; Scott
92 et al., 2004; Ignoul and Eggermont, 2005; Buey et al., 2017). For examples, the highly
93 conserved eukaryotic energy sensor AMPK (AMP-activated protein kinase)/SNF1 (Sucrose
94 Non-Fermenting kinase 1)/SnRK1 (SNF1 related kinase 1) is regulated by its γ -subunit
95 composed of four CBS domains in tandem (Polge and Thomas, 2007; Ramon et al., 2013;
96 Crozet et al., 2014). In mammals, AMP/ADP binding to the CBS domains of AMPK induces
97 a conformational change that stabilizes the phosphorylated activation loop of the protein by
98 upstream kinases (Hardie and Hawley, 2001; Ignoul and Eggermont, 2005; Xiao et al., 2011).
99 The Arabidopsis genome encodes 34 CDCPs each containing one or two pairs of CBS
100 domains that are generally closely associated with other functional protein domain(s). In these
101 proteins, CBS domains are expected to regulate the molecular function of other adjacent
102 domains. In contrast, the members of the CBSX subfamily of CDCP proteins carry a stand-
103 alone pair of CBS domains and are thus supposed to perform their regulatory function through
104 protein interactions (Kushwaha et al., 2009). In Arabidopsis, the six members of the CBSX
105 subfamily were proposed to be localized in several cellular compartments. Indeed, whereas
106 CBSX1 and CBSX2 were shown to be plastid targeted (Yoo et al., 2011; Jung et al., 2013),
107 CBSX3 was recently shown to be localized in mitochondria (Shin et al., 2020), CBSX4 is
108 predicted to be cytosolic and CBSX5 and CBSX6 are expected to be located in the
109 endoplasmic reticulum (Ok et al., 2012).

110 The two Arabidopsis plastidial CBSX, CBSX1 (AT4G36910) and CBSX2 (AT4G34120),
111 share 91% similarity and 74% identity in their amino acid sequences. Crystal structures of
112 Arabidopsis CBSX1 and CBSX2 were solved and showed that these two proteins form anti-
113 parallel (*head-to-tail*) homodimers exhibiting similar quaternary structures (Jeong et al.,
114 2013a; Jeong et al., 2013b).

115 To characterize CBSX1 and CBSX2 functions, Yoo *et al.* (2011) identified candidate protein
116 interactors using yeast 2-hybrid. Among them, were several chloroplast thioredoxins (TRX)
117 for which interactions were confirmed by *in vitro* pull-down assays and *in planta* bimolecular
118 fluorescence complementation (BiFC) experiments (Yoo et al., 2011; Jung et al., 2013). Both
119 CBSX1 and CBSX2 were shown to increase the activity of TRXm2, TRXf1, TRXx and
120 TRXy1 in a standard TRX activity assay based on bovine insulin reduction. These activities
121 were enhanced in presence of AMP (Yoo et al., 2011). Similarly, it was shown that CBSX3

122 enhances the *in vitro* activity of the mitochondrial TRXo1 and TRXo2 (Yoo et al., 2011; Shin
123 et al., 2020). Physiological functions of plastidial CBSX proteins were investigated in
124 transformed Arabidopsis over-expressing *CBSX1* and *CBSX2*. These plants exhibited a sterile
125 phenotype related to anther indehiscence. A defect in endothecium secondary cell wall
126 thickening during anther development was observed in over-expressors and linked to
127 insufficient reactive oxygen species (ROS) accumulation (Yoo et al., 2011; Jung et al., 2013).
128 *CBSX3* knockdown lines surprisingly presented a similar sterile phenotype related to an
129 anther indehiscence defect (Yoo et al., 2011; Jung et al., 2013; Shin et al., 2020). Plant
130 sterility of *CBSX1* and *CBSX2* over-expressors, on one hand, and *CBSX3* knockdown, on the
131 other hand, is supposedly linked to improper thioredoxin activities in plastids or in
132 mitochondria (Yoo et al., 2011; Jung et al., 2013; Shin et al., 2020).

133 Despite the previous in depth molecular characterization of the plastidial CBSX structures and
134 the demonstration of their interaction with TRX, the functional and physiological relevance of
135 CBSX regulatory role on TRX activities remains questioned. In this study, by evaluating
136 plastid CBSX regulation of TRX-dependent activities *in vitro* using two physiologically-
137 relevant targets of plastidial TRX, we show that *CBSX2* specifically inhibits TRX m activities
138 and that this effect is reversed by ATP and, to a lesser extent, by AMP. Adenylates impairing
139 direct CBSX-TRX interaction, we propose a model in which *CBSX2* specifically inhibits
140 reduced TRX m to maintain chloroplast energy status (ATP) for optimal plant growth during
141 acclimation to low temperature.

142 **RESULTS**

143 **Phylogenetic Analysis of AtCBSX**

144 To investigate relationships between the 6 Arabidopsis CBSX proteins, we constructed a
145 maximum likelihood phylogenetic tree from their full-length amino acid sequences. Our
146 analysis suggests that CBSX proteins that are localized in the same subcellular compartment
147 are closer in the phylogenetic tree than CBSX targeted to different locations (Figure S1). In
148 particular, the two closest Arabidopsis CBSX proteins, *CBSX1* and *CBSX2*, share 74% of
149 amino acid sequence identity (similarity 91%). They were both shown to be targeted to the
150 chloroplasts (Yoo et al., 2011; Jung et al., 2013). The closest protein of the plastidial CBSX
151 group, *CBSX3*, shares 26% of amino acid sequence identity with *CBSX2* (similarity 44%)
152 and is localized in mitochondria. *CBSX4*, (also known as AtPV42b) is homologous with
153 AtPV42a, a γ -type subunit of SnRK1 containing two CBS pairs (Fang et al., 2011).

154 Accordingly, it appears to be a non canonical CBSX standing apart in our phylogenetic tree.
155 This tree focused on the Arabidopsis CBSX subfamily is consistent with the wide
156 phylogenetic analysis made on the 34 CDCPs of *A. thaliana* and the 59 CDCPs of rice (*Oryza*
157 *sativa*) (Kushwaha et al., 2009).

158 **CBSX1 and CBSX2 are able to form homomers and heteromers in plastids**

159 We first confirmed the subcellular location of the chloroplast and mitochondrial CBSX
160 isoforms. Transiently transformed *Nicotiana benthamiana* leaves with CBSX-RFP fusions
161 were observed by confocal microscopy. Consistently with previous studies and predictions
162 (Yoo et al., 2011; Jung et al., 2013), fluorescence signals of full-length CBSX1-RFP and
163 CBSX2-RFP co-localized with the chlorophyll fluorescence of chloroplasts (Figure S2). In
164 contrast, the CBSX3-RFP fluorescence signal was observed as spots outside the chloroplasts
165 consistently with the recent finding from Shin *et al.* (2020) showing a mitochondrial
166 localization of CBSX3 (Figure S2).

167 Crystal structures of CBSX1 and CBSX2 previously showed that these two proteins form
168 homodimers with highly similar structures. The high similarity of their amino-acid sequences
169 suggests that they may also form heterodimers. We investigated this possibility in a yeast 2-
170 hybrid (Y2H) assay. CBSX1, CBSX2 and CBSX3 lacking their predicted organelle target
171 peptides were fused to Gal4 activation and DNA binding domains and expressed in relevant
172 Y2H strains. In a mating-based Y2H matricial assay, we showed that CBSX1 and CBSX2 can
173 form homomers as well as heteromers (Figure 1). In contrast, we did not identify any
174 interaction involving CBSX3, neither homomeric nor heteromeric.

175 To confirm these interactions in plant cells, we performed bimolecular fluorescence
176 complementation (BiFC) analysis. *Nicotiana benthamiana* leaves were transiently co-
177 transformed with full-length CBSX1 and CBSX2 fused at their C-termini to either the N-ter
178 moiety (nYFP) or the C-ter moiety (cYFP) of the yellow fluorescent protein. To enhance YFP
179 signals, plants were also co-transformed with HC-Pro, an inhibitor of gene silencing (Stephan
180 et al., 2011). Four days after transformation, specific chloroplastic YFP signals were observed
181 in both homomeric combinations (Figure 2). To test heteromerisation of CBSX1 and CBSX2,
182 two YFP combinations were tested. YFP signals were only observed when CBSX2-nYFP and
183 CBSX1-cYFP fusion proteins were co-expressed. The reciprocal combination did not give
184 any signal. Consistently with CBSX localization, signals were observed in plastids. For each
185 interaction signal, a spectral analysis of at least two spots was performed to confirm the YFP
186 fluorescence signature.

187 Altogether our results confirm that both CBSX1 and CBSX2 are targeted to plastid where
188 they form homomers as well as heteromers.

189 **CBSX2 inhibits the ability of TRX m to activate NADP-MDH and AMP modulates this**
190 **effect**

191 CBSX1 and CBSX2 proteins were previously found to activate TRX-dependent insulin
192 reduction (Yoo et al., 2011). Here, we investigated the ability of CBSX proteins to modulate
193 physiologically-relevant plastid TRX-dependent enzyme activities. To this aim, we produced
194 and purified recombinant his-tagged CBSX1 and CBSX2 in a bacterial expression system.
195 Untagged TRXs and TRX-regulated NADP-MDH were also obtained as previously described
196 (Collin et al., 2003). All proteins were produced without their target peptide. NADP-MDH
197 was previously shown to be efficiently activated *in vitro* by the members of the TRX m and
198 TRX f subfamilies (Collin et al., 2003) and its regulation by TRXf1, TRXm1 and TRXm2
199 was validated *in planta* (Thormählen et al., 2015; Thormählen et al., 2017). The plastid TRX-
200 regulated MDH uses NADPH as a cofactor to reduce oxaloacetate (OAA) into malate. Its
201 activation is strictly TRX dependent and requires the reduction of two constitutive regulatory
202 disulfide bonds, and a third transient disulfide (Issakidis et al., 1994; Ruelland et al., 1997).
203 Here, we tested the ability of five TRX isoforms (TRXm1, TRXm2, TRXm4, TRXf1 and
204 TRXf2) to activate MDH in presence or absence of CBSX. We incubated MDH with DTE-
205 reduced TRX, with or without addition of CBSX for 20 min prior to measuring MDH activity.
206 We checked that activation kinetics were linear and did not reach a plateau within 20 min of
207 incubation (Figure S3). We defined the MDH activation rate as the value of the initial activity
208 slope calculated after activation treatment. Our results show that CBSX1 does not have any
209 significant effect on the capacity of the five TRXs tested to activate NADP-MDH (Figure 3A-
210 E). In contrast, CBSX2 inhibits the enzyme activation by TRXm1 or TRXm2 or TRXm4
211 (Figure 3A-C), but not by TRXf1 or TRXf2 (Figure 3D,E). In presence of CBSX2 with
212 TRXm1, TRXm2 or TRXm4, NADP-MDH activation was reduced to 30-60% of the
213 maximum activation reached in absence of CBSX2 (Figure 3A-C). Because CBS domains
214 were shown to bind several adenosyl ligands (Ignoul and Eggermont, 2005) and, specifically,
215 CBSX2 structure was shown to be strongly modified upon AMP binding (Jeong et al., 2013a),
216 we tested the effect of this adenylate on the TRX limitation exerted by CBSX2. While TRX-
217 dependent MDH activation was not significantly affected by AMP (Figures 3 and S4), we
218 found that AMP limited the inhibitory effect of CBSX2 on TRX m (Figure 3A-C). Indeed,
219 TRX m-dependent MDH activation could reach 65-80% of its maximum in presence of

220 CBSX2 and AMP at a concentration of 1 mM, a concentration commonly used
221 experimentally to test regulation of CDCPs by adenylate ligands (Yoo et al., 2011; Jung et al.,
222 2013; Buey et al., 2017).

223 **CBSX2 directly regulates TRX activities**

224 Our results showed that CBSX2 selectively inhibits TRXs m but not TRXs f in their
225 capacities to activate NADP-MDH. They strongly suggested an inhibitory action of CBSX2
226 on TRX instead of a direct inhibition of MDH activity. To confirm these results, we took
227 advantage of a mutant form of NADP-MDH, the DMC (Double Mutation C-terminus)-MDH,
228 in which the two cysteines that form the C-terminal regulatory disulfide bond are substituted
229 by serines. The DMC-MDH has a basal enzyme activity without any activating treatment, but
230 reduced TRX is required to reach full activity (Issakidis et al., 1994). Without treatment, or in
231 presence of DTE alone, DMC-MDH exhibits *ca.* 25% of the activity reached after a 20 min
232 activation treatment in presence of TRXm1 (Figure 4). When DMC-MDH was incubated with
233 CBSX2 and DTE, its activity remained unchanged (Figure 4) confirming that CBSX2 does
234 not directly inhibit DMC-MDH activity. We also checked that AMP had no direct effect on
235 DMC-MDH activity (Figure S5). By contrast, DMC-MDH activation by TRXm1 or TRXm2,
236 like for the wild-type enzyme, was strongly impaired in presence of CBSX2, and AMP
237 limited this effect (Figure 4). Taken together our results strongly support a specific role
238 played by CBSX2 as a negative regulator of TRXs m, with AMP acting as a modulator.

239 **Adenosyl nucleotides differentially modulate TRX m inhibition by CBSX2**

240 Noticeably, we found that AMP alleviates the CBSX2 effect on TRXs m only partially in our
241 experimental conditions. The AMP concentration (1 mM) commonly used in this kind of
242 experiments corresponds to a concentration by far higher than reported AMP concentrations
243 in the chloroplast that do not exceed 1 μ M (Stitt et al., 1982). Thus, we also tested AMP at
244 lower concentrations, as well as other adenylate nucleotides, *e.g.* ADP and ATP prevailing in
245 the chloroplast (Figure 5). At 1 mM, we found that all adenylates could suppress the
246 inhibitory effect of CBSX2 (Figure 5), while they had no significant effect on TRXm1-
247 dependent activation of NADP-MDH (without CBSX) (Figure S4). At 1 mM, a physiological
248 concentration for ATP in the chloroplast, ATP could totally inhibit the effect of CBSX2
249 (Figure S6). We also tested MgATP, since *in vivo* 95-99 % of ATP is predicted to be
250 complexed with Mg²⁺, and we also found its strong effect on TRX m. Interestingly, by testing
251 lower concentrations of adenylate nucleotides, we could evidence that they have differential
252 effects on CBSX2 (Figure 5). Indeed, at 10 μ M, ATP, but neither AMP nor ADP, had an

253 effect, and at 50 μ M, AMP and ATP, but not ADP, restricted CBSX2 inhibition. At 1 mM,
254 ATP was significantly more efficient than ADP to limit CBSX2 inhibition. Thus, our data
255 suggest that AMP may not exert any effect on CBSX2 at physiologically relevant
256 concentrations. They also suggested that ADP may be much less efficient than ATP in
257 limiting CBSX2 effect on TRX, with estimated concentrations of ADP and ATP in the
258 chloroplast ranging from 0.5 to 0.8 mM and 0.8 to 1.2 mM, respectively (Stitt et al., 1982;
259 Voon et al., 2018). We also tested the effect of ATP together with ADP on the time course of
260 NADP-MDH activation in presence of CBSX2, at adenylate concentrations and ratios
261 corresponding to light and dark conditions prevailing in the chloroplast (Usuda, 1988) (Figure
262 S7). Again, CBSX2 effect was attenuated in presence of adenylates and, clearly, the effect
263 was more pronounced in the light mimicking condition compared to the dark mimicking
264 condition.

265 **CBSX2 inhibits TRX m-dependent reductive regeneration of 2-Cys PRX**

266 TRXs can regulate the activity of their targets (like NADP-MDH) and they can also provide
267 electrons to thiol-dependent peroxidases named peroxiredoxins (PRX). It was previously
268 shown that plastidial TRXs can reduce 2-Cys PRX *in vitro* with various efficiencies (Collin et
269 al., 2003; Collin et al., 2004; Bohrer et al., 2012). To extend CBSX function towards TRXs ,
270 we also tested other TRX isoforms that do not regulate NADP-MDH, *e.g.* TRXy1 and TRXx,
271 for their capacity to serve as reducing substrate for 2-Cys PRX (obtained as described in
272 Collin et al., 2003) in presence of CBSX. We found that PRX activities measured without
273 TRX (DTT alone) in absence and in presence of CBSX were very similar, showing that
274 neither CBSX1 nor CBSX2 has any direct effect on 2-Cys PRX reduction of tBOOH (an
275 alkyl-hydroperoxide) (Figure 6A). When combining PRX, TRX and CBSX proteins, we
276 found that the addition of CBSX1 had no effect on the peroxidase activity, and that TRXf1,
277 TRXy1 or TRXx were not affected by CBSX2 (Figure 6B-D). Similarly to its effect when
278 testing NADP-MDH activation, CBSX2 inhibited TRXm1-dependent reduction of the 2-Cys
279 PRX (Figure 6E). We also tested NTRC, a physiological substrate for this target, and found
280 that it was not significantly affected by CBSX2 (Figure 6F). As for NADP-MDH activation,
281 the addition of AMP restricted the inhibitory effect of CBSX2 on TRXm1 (Figure 7). These
282 results show that CBSX2 is able to specifically inhibit TRX m in serving as reducing
283 substrate for 2-Cys PRX and that, like in NADP-MDH activation, an adenylate nucleotide can
284 prevent this effect.

285 **Direct interaction between CBSX2 and TRXm1 proteins is modulated by adenosyl**
286 **ligands**

287 It was previously reported that CBSXs directly interact with TRXs (Yoo et al., 2011; Jung et
288 al., 2013; Shin et al., 2020). To validate these interactions and further investigate the effect of
289 adenosyl ligands, we performed pull-down assays with 6His-CBSXs and TRXm1 in presence
290 or absence of AMP or ATP. After incubation of TRXm1 and CBSX2 in reducing conditions
291 (presence of DTE), proteins were mixed with nickel affinity resin. After washings, they co-
292 eluted from the resin (Figure 8A). In contrast, interaction between CBSX2 and TRXm1 was
293 not observed when the incubation was performed in absence of a chemical reductant. Notably,
294 interaction was also abolished in presence of 1 mM AMP or ATP (Figure 8A,B). Similar
295 experiments were performed using 6His-CBSX1 and TRXm1, and no interaction was
296 detected (Figure 8B). Taken together these results show that CBSX2, but not CBSX1, is able
297 to interact with reduced TRXm1 in absence of ATP or AMP. These observations are
298 consistent with the specific inhibitory effect of CBSX2 on TRXm1 activities (NADP-MDH
299 activation and 2-Cys PRX reduction) and suggest that adenylyl ligands can modulate TRX m
300 inhibition by CBSX2 by preventing CBSX-TRX direct interaction. Notably, the absence of
301 effect of CBSX1 on TRXs could be linked to the lack of interaction between these two
302 proteins.

303 **The double mutant *cbsx1 cbsx2* is smaller and exhibits chlorophyll accumulation defects**
304 **at low temperature**

305 To investigate the role of CBSX in connection with TRX related functions *in planta*, we
306 characterized *cbsx1* and *cbsx2* Arabidopsis T-DNA insertion mutants. These mutants were
307 previously described in Yoo *et al.* (2011) and Jung *et al.* (2013), respectively, and did not
308 show any macroscopic phenotype at the rosette stage. Because we suspected functional
309 redundancy between the two CBSX plastid isoforms and found that they can form heteromers
310 *in vivo* (Figure 2), we crossed the corresponding single mutants to obtain the *cbsx1 cbsx2*
311 double mutant. In standard long day growth conditions, single and double mutants showed no
312 obvious phenotypes compared to wild-type (WT) plants (Figure 9A), as previously reported
313 under short day or continuous light (Yoo et al 2011; Jung et al 2013; Murai et al. 2021).
314 Because *CBSX1* and *CBSX2* genes were reported to exhibit an increased level of expression at
315 low temperature (ePlant database; (Waese et al., 2017)), the double mutant was germinated
316 and grown at 12°C. In this condition, the *cbsx1 cbsx2* double mutant rosettes were slightly
317 smaller and pale green in comparison with the WT (Col-0 ecotype) or single mutant plants

318 (Figure 9B). These differences were confirmed by comparing rosette fresh-weights and
319 chlorophyll contents of the double mutant, which were significantly decreased compared to
320 single mutants and WT plants (Figure 9E,F). These results suggest that both CBSX1 and
321 CBSX2 are required for normal growth and chloroplast functions at low temperature.

322 **The double mutant *cbsx1 cbsx2* shows altered P700 oxidation and reduction kinetics**

323 Since TRXs were proposed as specific regulators of the photosynthetic electron transport
324 (PET), we investigated whether PET was altered in *cbsx1 cbsx2*. We followed oxidation and
325 re-reduction of P700, the primary electron donor of photosystem I, by absorption
326 spectroscopy in the near infrared, in this double mutant, compared to WT and to TRX mutants
327 (double mutant *trxm1 trxm2* and single mutant *trxm4*). As shown in figure 10A, upon onset of
328 actinic light, the first fast transient oxidation level of P700 was higher in *cbsx1 cbsx2* than in
329 WT and *trxm1 trxm2*. Then a drop of the signal below the baseline, showing ferredoxin
330 reduction, was observed in all genotypes. This drop was followed by a multiphasic increase of
331 the signal until a steady state level of P700⁺ was reached. It is striking that in *cbsx1 cbsx2* this
332 steady state level was reached much faster than in the other genotypes. Illumination with far-
333 red light, exciting preferentially photosystem I, led to the same oxidation level in all
334 genotypes, with *trxm1 trxm2* reaching the maximum level of P700⁺ slower than WT and
335 *cbsx1 cbsx2*. Then far-red light was turned off and a saturating flash was given to achieve the
336 same maximum P700 oxidation level in all genotypes. We observed clear differences in the
337 oxidation kinetics between genotypes, showing that the pool of electron donors to
338 photosystem I available in *cbsx1 cbsx2* is smaller than in WT and *trxm1 trxm2*. This may be
339 interpreted as a sign of lower cyclic electron flow in *cbsx1 cbsx2*.

340 Next, we measured the rates of P700⁺ re-reduction after illumination of dark-adapted leaves
341 with far-red light. The re-reduction of P700⁺ after 1 min far-red illumination was much slower
342 in *cbsx1 cbsx2* than in WT, while in TRX mutants *trxm1 trxm2* and *trxm4* it was faster than in
343 WT as previously found in the same mutant lines (Thormählen et al., 2017; Courteille et al.,
344 2013) (Figure 10B and S8). This indicates a lower reduction state of the plastoquinone pool
345 after far-red illumination in *cbsx1 cbsx2* and can be interpreted as a lower cyclic flow in *cbsx1*
346 *cbsx2* compared with the other genotypes.

347 Taken together, both the P700 oxidation in actinic light and its re-reduction after far-red light
348 indicate that the electron transport chain is more oxidized in *cbsx1 cbsx2* and that in *cbsx1*
349 *cbsx2* lower cyclic flow takes place, both under actinic and far-red illumination.

350 **DISCUSSION**

351 Arabidopsis CBSX proteins were previously shown as regulatory interactors of chloroplastic
352 TRXs. However, their function was characterized using a non-physiological reduction assay.
353 Here, in order to understand the physiological function of CBSX1 and CBSX2 towards TRXs,
354 we tested the chloroplast TRX targets NADP-MDH and 2-Cys PRX. We show that CBSX2
355 specifically inhibits the activity of m-type TRXs, but does not have any effect on other
356 plastidial TRX isoforms (TRX f, TRX x and TRX y) and NTRC. In the same experimental
357 conditions, CBSX1 had no effect on tested TRX activities suggesting a different function for
358 this CBSX isoform in the chloroplast. Interestingly, despite its high sequence and structure
359 similarity with CBSX2, CBSX1 was shown to present some differences especially in the
360 relative angle between the monomers (Jeong et al., 2013b) that may be responsible for distinct
361 functionalities between the two isoforms. However, we cannot totally exclude that our
362 CBSX1 protein preparation, although obtained following exactly the same methodology as for
363 CBSX2, could be inactive.

364

365 We found that both ADP and ATP are able to alleviate CBSX2 inhibition of TRX m, at
366 physiologically relevant concentrations, with a stronger effect of ATP. In chloroplasts, ATP is
367 produced by the thylakoid membrane ATP synthase complex from ADP and inorganic
368 phosphate. Upon illumination, a rapid increase in the level of ATP accompanied by a marked
369 decrease in AMP and a slight decrease in ADP were observed (Santarius and Heber, 1965;
370 Kobayashi et al., 1979; Voon et al., 2018). This raise in ATP levels in chloroplasts in the light
371 and the higher efficiency of ATP in modulating CBSX effect on TRX suggest that ATP is the
372 major ligand of CBSX2 in plant cells. Generally, CDCPs, like AMPK γ , that bind AMP or
373 ATP are affected by both but exhibit differential affinity (Scott et al., 2004). Although crystal
374 structure analysis suggested that CBSX2 cannot bind ATP (Jeong et al., 2013a), our data
375 clearly show a modulating effect of ATP onto CBSX2 functions towards TRXs m. ATP
376 probably binds to CBSX2 and ATP-bound CBSX2 crystal structure might validate this
377 possibility in the future.

378 We found a relationship between protein-protein as well as ligand-protein interactions and
379 functional inhibitory effects, allowing us to propose a model integrating molecular
380 interactions in the mechanism of TRX m inhibition by CBSX2 (Figure 11). When ATP
381 concentration is low, CBSX2 is able to interact with reduced TRX m. This interaction inhibits
382 TRX m ability to reduce its targets. Since CBSX proteins are devoid of any Cys residue the
383 hypothesis of a competition between CBSX2 and targets for electron transfer from TRX can

384 be ruled out. Instead, a competition between CBSX2 and a TRX target may occur at the
385 surface of TRX, or interaction of CBSX2 with TRX m may induce a conformational change
386 of the TRX that would be unfavorable for electron transfer and/or target interaction. The
387 CBSX2 structure in complex with AMP, solved at 2.2Å resolution, appeared to be
388 approximately flat, with a strong reshaping of the protein upon AMP binding (Jeong et al.,
389 2013a). This could be also hypothesized for ATP binding. Thus, when ligand concentration is
390 high, CBSX2 protein would undergo a conformational change that may prevent interaction
391 with TRX. Our model based on direct protein-protein interaction would explain the specificity
392 of the inhibition of TRX m by CBSX2.

393
394 *In planta*, by measuring leaf NADP-MDH activity (extractable and maximal) and 2-Cys PRX
395 redox state (monomer/dimer status and over-oxidation), we found no clear difference in *cbx*
396 mutant leaves compared to wild-type plants cultivated at control or at low temperature (Figure
397 S9). This result suggests that in our growth conditions these two targets might be principally
398 regulated by TRX isoforms other than TRXs m, or NTRC, as already reported *in vitro* and *in*
399 *vivo* (Collin et al., 2003; Pulido et al., 2010; Yoshida et al., 2015; Pérez-Ruiz et al., 2017).
400 Recent genetic studies have allowed investigating specifically the roles of TRXs m *in vivo*
401 and point to their role in regulating the proton motive force (pmf). pmf primarily drives ATP
402 synthesis and is a prerequisite for light-dependent activation of ATP synthase (CF1- γ
403 reduction) by TRXs m and f (Junesch and Gräber, 1987; Sekiguchi et al., 2020). TRX m1 and
404 m2 would be necessary for full activation of photosynthesis during the high light periods
405 where elevated levels of reduced photosystem I (PSI) acceptors favor cyclic electron transport
406 (CET) (Thormählen et al., 2017). By recycling electrons from ferredoxin to the thylakoid
407 plastoquinone (PQ) pool via PQ reductases, PSI-CET allows maintaining the appropriate pH
408 range of the thylakoid lumen contributing to the Δ pH causal to the pmf that drives ATP
409 synthase. Since ATP synthesis occurs without production of NADPH, PSI-CET is important
410 to maintain an optimal ATP/NADPH ratio to meet metabolic demand and thereby optimal
411 plant growth (Yamori and Shikanai, 2016). Notably, when the *trxm1_m2_m4* triple mutant
412 was compared to the wild-type, Okegawa and Motohashi (2015) found that the ATP level was
413 higher in the light, and the initial rate of light-dependent CF1- γ reduction was slowed down
414 (Sekiguchi et al., 2020). Data obtained in Arabidopsis show that both PQ reductase pathways,
415 namely the Proton Gradient Regulation 5 (PGR5)/PGRL1 (PGR-like 1) complex and the
416 NADH dehydrogenase-like complex (NDH), contribute to supply sufficient acceptors from
417 PSI (Shikanai, 2016). While a predominant role is played by the PGR5/PGRL1 pathway in

418 normal growth conditions (Nakano et al., 2019), NDH is believed to protect the
419 photosynthetic apparatus at chilling stress under low irradiance when ΔpH is low (Yamori et
420 al., 2011; Yamori et al., 2015). Courteille *et al.* (2013) reported that Tobacco TRX m
421 overexpressing plants are characterized by a down regulation of PSI-CET via the NDH
422 pathway while NDH-dependent PQ reduction was up-regulated in Arabidopsis mutant plants
423 specifically lacking TRXm4. It was proposed that TRXs m may promote reduction of dimeric
424 PGRL1 to its monomeric activated form (Hertle et al., 2013) and interaction of TRXm1 with
425 PGRL1 has been shown *in planta* (Nikkanen et al., 2018). Recently, Okegawa and Motohashi,
426 confirmed the regulation of the PGR5/PGRL1 complex by m-type TRXs and reported that
427 TRXm4 downregulates the PGR5/ PGRL1-dependent pathway via a direct interaction with
428 PGRL1 (2020). Here, we found that, compared to wild-type, TRX m lacking plants (*trxm1m2*
429 double mutant and *trxm4* single mutant) exhibited a faster P700⁺ reduction (Figure 10B and
430 Figure S9), similarly to previously reported data (Courteille et al., 2013). On the contrary, the
431 *cbx1 cbx2* mutant showed a slower reduction indicative of decreased oxidation of the PQ
432 pool favorable for PSI-CET. Thus, CBSX affects P700 photo-oxidation reduction cycle in
433 PSI. By avoiding accumulation of electrons in the PQ pool, CBSX would allow maintaining a
434 pH range in the luminal space of the thylakoid membrane appropriate for ATP synthesis
435 (Miyake, 2020).

436 At low temperature, transcriptomics databases indicate a higher expression level of *CBSX1*
437 and *CBSX2* genes (Waese et al., 2017) while transcripts abundance for TRXm1, TRXm2 and
438 TRXm4 are decreased (Dreyer and Dietz, 2018). When we investigated the *cbx1 cbx2*
439 mutants growth at low temperature (12°C), and under a weak illumination (60 μmol
440 $\text{photons}\cdot\text{m}^{-2}\cdot\text{s}^{-1}$) to avoid photoinhibition, we found that the double mutant exhibited growth
441 and chlorophyll accumulation defects in these conditions. These phenotypes may be caused
442 by a suppression of PSI-CET. Noticeably, PSI-CET is enhanced in pea leaves by chilling
443 (Cornic et al., 2000), as in rice, where NDH-dependent cyclic electron flow plays a
444 substantial role for photosynthesis and plant growth at low temperature (Yamori et al., 2011).
445 Moreover, both pathways of PSI-CET protect tomato leaves against photoinhibition when
446 exposed to chilling stress (Wang et al., 2020).

447 Notably, impaired growth and decreased chlorophyll content were found in Tobacco plants
448 over-expressing TRX m (Rey et al., 2013). Da *et al.* (2017) reported a high pmf in TRX m-
449 deficient Arabidopsis plants and Thormälen *et al.* (2017) found that in *trx m1m2* mutants PSI
450 yield was enhanced and accompanied by an increased oxidation of the PQ pool, indicative of
451 PSI-CET stimulation. Thus, in our chilling growth conditions (low temperature and low light

452 intensity), we believe that no damage of photosynthetic membranes occurred (no
453 photoinhibition) and that a high PSI-CET was necessary to sustain ATP homeostasis and
454 plant growth. Based on previous studies on TRXs m, this would imply alleviation of their
455 negative regulation exerted on PSI-CET, and, based on the present work, we hypothesize that
456 this would implicate CBSX proteins.

457 Interestingly, a recent work reported the role played by adenylates to balance the “plastid
458 energy budget”, supporting the view that PSI-CET is activated under conditions where
459 stromal ATP is low, but is downregulated as ATP levels build up, allowing for effective ATP
460 homeostasis (Fisher et al., 2019). Accordingly, we propose a model (Figure 12) in which
461 CBSX2, acting as a sensor of the chloroplast energy status, would specifically decrease
462 reduced TRX m activity when ATP concentration is low. This would consequently decrease
463 TRX m-dependent negative regulation of PSI-CET to allow a higher pmf-driven ATP
464 production, since TRXs f are not affected by CBSX2 and efficiently activate ATP synthase.

465 Overall, present findings reveal an ATP sensing mechanism involving cystathionine- β -
466 synthase domain protein and thioredoxin possibly acting for optimal ATP homeostasis in the
467 chloroplast.

468

469

470 MATERIALS AND METHODS

471 Plants Materials

472 *Arabidopsis (Arabidopsis thaliana)* T-DNA insertion mutants *cbsx1* (Gabi_050D12), *cbsx2*
473 (Salk_136934), *trxm1 trxm2* (Salk_087118_ and Salk_123570), *trxm4* (Salk_0 532538) were
474 previously described in Yoo *et al.* (2011), Jung *et al.* (2013), Thormählen *et al.* (2017), and
475 Courteille *et al.* (2013), respectively. They were obtained from the NASC (Nottingham
476 *Arabidopsis* Stock Centre) (Scholl et al., 2000), and controlled by PCR genotyping (sequence
477 of primers used can be found in Table S1). Plants are sown and grown under long days
478 conditions (16h light/day) at 20°C or 12°C constant temperature. Light intensity was 60 μmol
479 $\text{photons.m}^{-2}.\text{s}^{-1}$ (tubular fluorescent lamps: Sylvania Lynx-LE 840, white light) at the level of
480 the leaves.

481 Phylogenetic Analysis

482 We used TAIR10 models to determine the full-length amino acid sequences of the six
483 *Arabidopsis* CBSX: CBSX1 (AT4G36910), CBSX2 (AT4G34120), CBSX3 (AT5G10860),

484 CBSX4 (AT1G80090), CBSX5 (AT4G27460) and CBSX6 (AT1G65320). The phylogenetic
485 tree was inferred using the Maximum Likelihood method based on the Jones-Taylor-Thornton
486 (JTT) matrix-based model (Jones et al., 1992), bootstraps: 1000. Analysis were conducted on
487 MEGA7 (Kumar et al., 2016).

488 **Yeast 2-Hybrid**

489 *CBSX1* (72-236), *CBSX2* (72-238) and *CBSX3* (16-206) truncated ORF were amplified and
490 cloned into the pDONR207 vector using Gateway BP Clonase enzyme (Invitrogen). Primers
491 (ORF_intern + ORF_stop, sequences can be found in Table S1) were designed to amplify
492 ORF encoding mature proteins lacking their putative target peptide (prediction by TargetP 1.1
493 (Nielsen et al., 1997; Emanuelsson et al., 2000)). *CBSX* ORF were then subcloned into
494 pDEST-AD-CYH2 and pDEST-DB destination vectors (Dreze et al., 2010) using Gateway
495 LR Clonase enzyme (Invitrogen) according to manufacturer's instructions. Y8800 MAT α and
496 Y8930 MAT α yeast strains (James et al., 1996) were transformed with AD-ORF and DB-
497 ORF, respectively. Yeast mating and selection were performed according to the InterATOME
498 platform pipeline as previously described in Monachello *et al.* (2019). As positive interacting
499 protein control we used DB-mNUWA and AD-mDYW2 (Guillaumot et al., 2017).

500 **Bimolecular Fluorescence Complementation and Subcellular localization**

501 *CBSX1* (1-236), *CBSX2* (1-238) and *CBSX3* (1-206) full length ORF were amplified and
502 cloned into the pDONR207 vector using Gateway BP Clonase enzyme (Invitrogen). Primers
503 (ORF_start + ORF_end, sequences can be found in Table S1) were designed to amplify ORF
504 without stop codon allowing C-terminal fusion after Gateway LR transfert into pGreen-0229-
505 RFP, pBiFC1 or pBiFC4 destination vectors (Boussardon et al., 2012). For subcellular
506 localization, C58C1 pSOUP *Agrobacterium tumefaciens* cells were transformed with pGreen-
507 0229-RFP vectors. For Bimolecular Fluorescence Complementation, C58C1 pMP90
508 *Agrobacterium tumefaciens* cells were transformed with pBiFC1 and pBiFC4 vectors. For all
509 experiments leaves of *Nicotiana benthamiana* were co-infiltrated with agrobacteria containing
510 required vectors and the silencing inhibitor HC-Pro (Stephan et al., 2011). Leaves were
511 observed 4 days after transformation using a Zeiss LSM880 confocal scanning microscope
512 (Zeiss, Germany) with a Plan-APO 20x/0.8 objective (and a zoom 2x). The microscope was
513 equipped with a 514nm laser Argon set to 5% power for YFP and chlorophyll
514 autofluorescence excitation in BiFC experiments and a 561nm laser line set to 3% or 15%
515 power depending on the observed CBSX protein for RFP and chlorophyll autofluorescence
516 excitation in subcellular localization experiments. Green (YFP or RFP) and magenta

517 (chlorophyll) channels fluorescence emissions were collected using a sequential mode with
518 variable beam splitter between 526-615 nm, 562-624 nm and 674-735 nm respectively, and
519 with a 32-PMTs GaAsP detector. The pinhole was set to 0.72 airy unit. The detectors offset
520 and gain were set to a small number of zero-value pixels and to optimize the dynamic range
521 while ensuring minimal saturated pixels and were kept for all acquisitions of the same
522 experiment. Images were acquired using ZEN Dark software (Zeiss, Germany) and processed
523 using ZEN lite (Zeiss, Germany). Image acquisition and image analysis were performed using
524 the IPS2 imaging facility platform.

525 **Protein Production and Purification**

526 *CBSX1* (72-236) and *CBSX2* (72-238) ORF in pDONR207 were subcloned into the
527 expression vector pDEST17 (Invitrogen) using Gateway LR Clonase enzyme (Invitrogen)
528 according to manufacturer's instructions. Protein production in *Escherichia coli* BL21 cells
529 was induced overnight at 30°C in LB medium containing 100 µg/mL carbenicilline and 400
530 µM IPTG. Bacteria lysis was performed in 30 mM Tris pH7.9 containing protease inhibitor
531 (complete Mini EDTA-free Roche®) using a French press. Proteins were purified by affinity
532 chromatography using a nickel column (GE healthcare® His-trap HP 1mL). Column washing
533 was performed with 30 mM Tris pH 7.9 containing 20 mM imidazole. Proteins elution was
534 performed with 30 mM Tris pH 7.9 containing 200 mM imidazole. Eluted proteins were
535 dialysed and concentrated in 30 mM Tris pH 7.9 using Amicon columns (Sigma Amicon
536 ultra-4 Z740191-8EA 30K). All TRX and 2-Cys PRX proteins were produced as previously
537 described in Collin *et al.* (2003; 2004). NTRC was obtained as described in Bohrer *et al.*,
538 2012. Fully activated wild-type MDH and mutant DMC-MDH recombinant enzymes,
539 obtained as previously described in Issakidis *et al.* (1994), had a specific activity (u/mg) of
540 368 +/- 42 and 386 +/- 25, respectively. 2-Cys PRX exhibited a K_{cat} of 179 +/- 17 s⁻¹ with
541 TRXx as reducing substrate. All these values being very close to those previously reported
542 (Issakidis *et al.*, 1994; Collin *et al.*,2003) certified that appropriate purified protein
543 preparations were used for the present study.

544 **MDH activity**

545 MDH (0.24 g/L) was activated by incubation with 10 mM DTE-reduced TRX with the
546 eventual addition of 30 µM CBSX and 1 mM AMP or ATP, as indicated, in 30 mM Tris
547 pH7.9 at 21°C. TRX concentration was 10 µM for all TRX excepted TRX f1 used at 1 µM. 3
548 µL aliquots of reaction medium were periodically withdrawn and added to 200 µL of 30°C
549 pre-heated reaction medium (for wild-type MDH: 160 µM NADPH, 750 µM OAA, 30 mM

550 Tris pH7.9 ; for DMC-MDH: 160 μ M NADPH, 1 mM OAA, 30 mM Tris pH7.9).
551 Experiments with MgATP were performed by incubation with 1 mM ATP and 10 mM
552 MgCl₂. The MDH activity was measured by following the NADPH consumption at 340 nm
553 during 1 min in a Tecan infinite m200 PRO plate reader. Each experiment has been repeated
554 at least twice, with three to four technical replicates in each experiment. MDH activities
555 (initial velocities) were estimated as the slopes calculated during 20 seconds. When the
556 coefficient of variation of the estimated slope was higher than 15%, we discarded the data.
557 We defined TRX activity as the MDH activity after 20 minutes of activation. Statistical
558 analysis of MDH activity dataset was performed with a linear model taking into account TRX,
559 CBSX and adenylate effects.

560 **PRX activity**

561 0.4 mM of tBOOH (tert-butyl hydroperoxide) was reduced by 15 μ M 2-Cys PRX A, 15 μ M
562 of 0.5 mM DTE-reduced TRX, 45 μ M CBSX and 1 mM AMP in 100 mM Tris pH7.9.
563 Unreduced tBOOH in 10 μ L aliquots was periodically quantified at 560 nm using the FOX
564 coloration procedure described in Collin *et al.* (2004). CBSX direct effect on PRX was
565 assayed in presence of 1 mM DTE.

566 **Analysis of chlorophyll content**

567 Chlorophyll quantification was performed by acetone extraction on 50 mg fresh rosette leaf as
568 previously described in Sumanta et al. (2014).

569 **P700 absorption**

570 The redox state of P₇₀₀ was monitored by following differences of the 875 nm and 830 nm
571 transmittance signals using a DUAL-PAM-100 (Walz, Effeltrich, Germany). When P700
572 oxidation was measured with actinic light, plants were kept prior to the measurements in the
573 light in the growth chamber so that the Calvin-Benson cycle enzymes were active. When the
574 pool of electron donors was measured by following P700⁺ re-reduction after far-red
575 illumination, plants were kept in the dark prior to the measurement to ensure inactive Calvin-
576 Benson cycle enzymes. The acquisition rate was set to 1 ms.

577 **Statistical analysis**

578 All statistical analyses were conducted on R (version 3.2.5). To analyze each dataset, we used
579 ANOVA with several factors and when necessary statistical interactions were considered. To
580 control the family-wise error rate, p-values were adjusted using the Bonferroni procedure. A
581 difference was considered significant when its adjusted p-value was lower than 0.05.

582 For the MDH activities dataset with the four TRXs, two CBSXs and AMP, the mean is
583 defined as the single TRX, CBSX and AMP effects, their pairwise interactions and the third
584 order interaction.

585 For the DMC-MDH activities dataset, the mean is defined as the single TRX, CBSX and
586 AMP effects and the interaction between CBSX and TRX. This model is the most complete
587 according to the experimental design.

588 For the MDH activities dataset with AMP, ATP and MgATP, the mean is defined as the
589 single CBSX and ligand effects and their interaction.

590 For MDH activities dataset with AMP, ADP and ATP, the mean is defined as the single
591 CBSX and ligand effects and their interaction.

592 For the MDH activities dataset with AMP and ATP ranging from 1 μ M to 1mM, the mean is
593 defined as the single CBSX and ligand effects and their interaction.

594 For the PRX activities dataset with CBSX2 and AMP effects on TRX m1, the mean is defined
595 as the single CBSX and AMP effects and their interaction.

596 For the rosette fresh-weight and chlorophyll content datasets, the mean is defined as the
597 genotype effect.

598 For P700⁺ datasets, the mean of half-time reduction is defined as the genotype effect.

599 For *in planta* MDH initial and maximal activities dataset, the mean is defined as the genotype
600 effect.

601 **Pull-down**

602 Purified 6His-CBSX2 protein (500 μ g) was incubated with TRX m1 (285 μ g) in 350 μ L assay
603 buffer (1x PBS, \pm 1 mM DTE \pm 1 mM AMP \pm 1 mM ATP) for 1h at room temperature. After
604 adding 50 μ L of Ni-NTA agarose beads (Qiagen) and incubation for 1h at room temperature,
605 beads were washed 3 times with 500 μ L of assay buffer. Proteins were eluted with 200 mM
606 imidazole. Immunoblotting was performed with mouse anti-6HIS (Roche® #11922416001)
607 and rabbit specific anti-TRXm1 (generated against AtTRXm1 recombinant protein,
608 Genosphere Biotechnologies) as primary antibodies, and anti-mouse (Sigma A5906) and anti-
609 rabbit (Sigma A6154) as HRP-conjugated secondary antibodies. Blot revelation was
610 performed with the BIORAD Clarity™ Western ECL Substrate on a BIORAD® Chemidoc
611 ISV0025.

612

613 **ACCESSION NUMBERS**

614 *CBSX1* (AT4G36910), *CBSX2* (AT4G34120), *CBSX3* (AT5G10860), *CBSX4* (AT1G80090),
615 *CBSX5* (AT4G27460), *CBSX6* (AT1G65320), *TRXM1* (AT1G03680), *TRXM2* (AT4G03520),
616 *TRXF1* (AT3G02730), *TRXF2* (AT5G16400), *TRXX* (AT1G50320), *TRXY1* (AT1G76760),
617 *NUWA* (AT3G49240) and *DYW2* (AT2G15690).
618 *2-CYS PRXA* (AT5G58330), *NADP-MDH* (AT3G11630).

619 **SUPPLEMENTAL DATA**

620 Table S1: Primers used in the study.

621 Figure S1: *Arabidopsis thaliana* CBSX phylogenetic tree.

622 Figure S2: Subcellular localization of CBSX1, CBSX2 and CBSX3.

623 Figure S3: NADP-MDH activation kinetics.

624 Figure S4: Test of direct effect of adenylates on TRXm1-dependent NADP-MDH activation.

625 Figure S5: Effect of AMP on mutant DMC-MDH activity.

626 Figure S6: Effect of ATP on CBSX2 towards TRXm1-dependent NADP-MDH activation.

627 Figure S7: Effects of ATP together with ADP at concentrations and ratios mimicking light
628 and night conditions on CBSX2 towards TRXm1-dependent NADP-MDH activation.

629 Figure S8: P700⁺ reduction.

630 Figure S9: TRX targets in the context of CBSX mutations.

631

632 **Funding information:** K.B. research was supported by a French Ph. D. fellowship from
633 “Ministère de la Recherche et de l’Enseignement Supérieur”. D.G. research was supported by
634 a post-doctoral fellowship from a French State grant (Saclay Plant Sciences, reference n°
635 ANR-17-EUR-0007, EUR SPS-GSR) managed by the French National Research Agency
636 under an Investments for the Future program (reference n° ANR-11-IDEX-0003-02). The
637 IPS2 and the I2BC benefit from the support of the Labex Saclay Plant Sciences-SPS (ANR-
638 17-EUR-0007). This work was supported by the French Infrastructure for Integrated
639 Structural Biology (FRISBI; grant number ANR-10-INSB-05).

640 **ACKNOWLEDGMENTS**

641 We greatly thank Marie-Laure Martin-Magniette who helped us with statistical analysis. We
642 are grateful to Cécile Raynaud who provided us with the *Agrobacterium* strain containing the
643 HC-pro silencing inhibitor. We would also like to thank Myroslawa Miginiac-Maslow for
644 constructive criticism of the manuscript.

645 **FIGURE LEGENDS**

646 **Figure 1.** Protein interactions between Arabidopsis CBSX isoforms assayed by yeast 2-
647 hybrid.

648 Interactions were tested using a mating-based Y2H matricial assay with AD fusions on the
649 horizontal axis and the DB fusions on the vertical axis. In the “H₂O” row and column, yeast
650 cells were replaced by water; in the “Ø” row and column, mating was performed with yeasts
651 transformed with an empty vector. As a positive interaction control, we used DB-mNUWA
652 and AD-mDYW2 (Guillaumot et al., 2017). Interactions were tested on selective medium
653 without histidine.

654 **Figure 2.** *In planta* protein interactions between CBSX isoforms assayed by BiFC.

655 BiFC of YFP in transiently transformed *Nicotiana benthamiana* leaves. Left column, YFP
656 fluorescence signal. Middle column, chlorophyll fluorescence signal. Right column, merge of
657 fluorescent signals. Fluorescence spots confirmed as YFP fluorescence signals by spectral
658 analysis are indicated by white arrows. Observations were performed four days after
659 transformations. Bars=10 µm.

660 **Figure 3.** Effect of CBSX1 and 2 on TRX capacity to activate wild-type NADP-MDH, and
661 effect of AMP.

662 NADP-MDH activation was measured after 20 min incubation at room temperature in
663 presence of 10 µM TRX (except TRXf1 at 1 µM) and 10 mM DTE. 100% activation rate
664 corresponds to the activation with DTE-reduced TRX (without CBSX and AMP). (A)
665 TRXm1 (mean SA = 372 u/mg), (B) TRXm2 (mean SA = 314 u/mg), (C) TRXm4 (mean SA
666 = 383 u/mg), (D) TRXf1 (mean SA = 432 u/mg) and (E) TRXf2 (mean SA = 340 u/mg).
667 CBSX1/2 and AMP final concentration were 30 µM and 1 mM, respectively. Values are
668 means ± SD (n=4). Bars with different letters correspond to significantly different values. *P* <
669 0.05. SA: specific activity of NADP-MDH at maximal activation (100%) expressed in units
670 (u: µmole NADPH oxidized per min) per mg of enzyme.

671 **Figure 4.** Effect of CBSX2 on mutant DMC-MDH activity and TRXm-dependent activation,
672 and effect of AMP.

673 DMC-MDH activation was measured after 20 min incubation at room temperature in presence
674 of DTE alone (Ø TRX), or DTE + TRXm1, or DTE + TRXm2. 100% activation rate
675 corresponds to the maximal activation of DMC-MDH by DTE-reduced TRXm1/2 (without
676 CBSX and AMP). Mean specific activity of DMC-MDH at maximal activation (100%) were
677 391 u/mg and 382 u/mg, with TRXm1 and TRXm2, respectively. Values are means ± SD

678 (n=4). TRXm1/2, CBSX2 and AMP were at a final concentration of 10 μ M, 30 μ M and 1
679 mM, respectively. Bars with different letters correspond to significantly different values. $P <$
680 0.05.

681 **Figure 5.** Effects of adenylates on CBSX2 inhibition of TRXm-dependent NADP-MDH
682 activation.

683 Wild-type MDH activation was measured after 20 min incubation in presence of DTE-
684 reduced TRXm1 (10 μ M) with CBSX2 (30 μ M) and 0, 1, 10, 50 or 1000 μ M of AMP, ADP
685 or ATP. Values are means \pm SD (n=4-6). Bars with different letters correspond to
686 significantly different values. $P <$ 0.05.

687 **Figure 6.** Effect of CBSX1 and 2 on 2-Cys PRX activity.

688 Time course of tBOOH reduction by 2-Cys PRXA in presence of DTT alone (black curves),
689 DTT-reduced TRX (grey curves), DTT-reduced TRX and CBSX1 (blue curves) or CBSX2
690 (orange curves). (A) DTT alone; (B) DTT + TRXx; (C) DTT + TRXf1; (D) DTT + TRXy1;
691 (E) DTT + TRXm1; (F) DTT + NTRC. The values are means \pm SD (n=3).

692 **Figure 7.** Effect of 1 mM AMP on CBSX2 towards TRXm1-dependent 2-Cys PRX activity.
693 2-Cys PRX activities were defined as the tBOOH reduction kinetic slope between 2 and 10
694 min and were normalized to the activity in the control condition (without CBSX and AMP)
695 considered as 100%. The values are means \pm SD (n=3). Bars with different letters correspond
696 to significantly different values. $P <$ 0.05.

697 **Figure 8.** Pull-down assays with CBSX and TRXm proteins.

698 Pull-down of His-CBSX and TRXm1 in absence or presence of DTE, AMP and ATP. (A)
699 Impact of 1 mM AMP and DTE on CBSX2-TRXm1 interaction. (B) Impact of 1 mM ATP or
700 1 mM AMP on CBSX-TRXm1 interaction. Input corresponds to proteins initially mixed
701 before incubation with His-affinity agarose beads. Output corresponds to proteins eluted (after
702 washes) from the resin by 200 mM imidazole. The bracket indicates an unspecific low
703 molecular weight signal obtained using anti-TRXm1 antibodies on CBSX preparations.

704 **Figure 9.** *cbsx* mutant phenotypes.

705 (A) Representative 5-week old plants grown in long day conditions at 20°C (bar= 1cm). (B)
706 Representative 11-week old plants grown in long day conditions at 12°C (bar= 1cm). Plant
707 images were digitally extracted for comparison. (C) and (D) Plants grown at control
708 temperature. (E) and (F) Plants grown at low temperature. (C) and (E) Rosette fresh weight,
709 values are means \pm SD (n=10), *: $P <$ 0.01. (D) and (F) Chlorophyll (Chl) a and b contents,
710 and Chla/Chlb ratios, values are means \pm SD (n=10). *: $P =$ 0.02.

711 **Figure 10.** P700 measurements on leaves of wild-type plants and Trx m- and CBSX-deficient
712 mutants.

713 The redox state of the PSI primary donor P700 was monitored through the changes in
714 absorbance at 830 versus 875 nm. (A) Representative curves are shown of plants kept at
715 growth light intensity; WT: black, *cbsx1cbsx2*: red, *trxm1trxm2*: green. Leaves were
716 illuminated with actinic red light, AL ($I=830 \mu\text{mol photons}\cdot\text{m}^{-2}\cdot\text{s}^{-1}$) to oxidize P700 until a
717 steady state was reached. Then far-red light, FR, was switched on. To achieve the maximum
718 oxidation state a saturating flash, SF, was given at the end of the FR illumination. (B) Half-
719 time of P700⁺ reduction after FR illumination of dark-adapted plants. The traces of the
720 kinetics are shown in Figure S8. Bars with different letters correspond to significantly
721 different values between genotypes. $P < 0.05$.

722 **Figure 11.** Model of TRX activity regulation by CBSX2.

723 CBSX2 homodimer (yellow disc) is unable to interact with oxidized TRX m (green circle)
724 (A), but is able to interact with reduced TRXm and inhibits TRX m capacity to reduce its
725 target (blue circle) (B). A conformational change of CBSX2 induced by adenosyl ligand (red
726 circle) binding provokes the release of TRXm-CBSX2 interaction allowing TRXm to act on
727 its target (C).

728 **Figure 12.** Model for functional relationship between CBSX and TRX in the context of ATP
729 homeostasis in the chloroplast.

730 In the proposed model, when ATP level is low (A), CBSX can interact with TRX m,
731 impeding its negative regulation of PSI-CET, which is primarily coupled to the generation of
732 the proton motive force driving the synthesis of ATP by the thylakoid ATP synthase complex.
733 When ATP level increases (B), ATP binds to CBSX, preventing interaction with TRX m and
734 allowing down-regulation of the PSI-CET and thereby lowering ATP synthesis.
735 Electron and proton transfers are shown by red and blue arrows, respectively. Abbreviations
736 are : PSI/II, photosystem I/II; Cyt b6/f, cytochrome b6/f complex; Fd, ferredoxin; FNR,
737 ferredoxin-NADP reductase; FTR, ferredoxin/thioredoxin reductase; TRX, thioredoxin;
738 CBSX, cystathionine- β -synthase domain protein; PQ, plastoquinone; PQH2, plastoquinol; PC,
739 plastocyanin; PSI-CET, cyclic electron transport around PSI; CF0 and CF1, coupling factor 0
740 and 1 of chloroplast ATP synthase, respectively.

741 REFERENCES

742 **Baier M, Dietz K-J** (2005) Chloroplasts as source and target of cellular redox regulation: a
743 discussion on chloroplast redox signals in the context of plant physiology. *J Exp Bot* **56**:

744 1449–1462

745 **Bateman A** (1997) The structure of a domain common to archaebacteria and the
746 homocystinuria disease protein. *Trends Biochem Sci.* doi: 10.1016/S0968-
747 0004(96)30046-7

748 **Bohrer A-S, Massot V, Innocenti G, Reichheld J-P, Issakidis-Bourguet E, Vanacker H**
749 (2012) New insights into the reduction systems of plastidial thioredoxins point out the
750 unique properties of thioredoxin z from Arabidopsis. *J Exp Bot* **63**: 6315–6323

751 **Boussardon C, Salone V, Avon A, Berthome R, Hammani K, Okuda K, Shikanai T,**
752 **Small I, Lurin C** (2012) Two interacting proteins are necessary for the editing of the
753 NdhD-1 Site in Arabidopsis plastids. *Plant Cell* **24**: 3684–3694

754 **Buey RM, Fernández-Justel D, Marcos-Alcalde Í, Winter G, Gómez-Puertas P, de**
755 **Pereda JM, Luis Revuelta J** (2017) A nucleotide-controlled conformational switch
756 modulates the activity of eukaryotic IMP dehydrogenases. *Sci Rep* **7**: 2648

757 **Collin V, Issakidis-Bourguet E, Marchand C, Hirasawa M, Lancelin J-M, Knaff DB,**
758 **Miginiac-Maslow M** (2003) The Arabidopsis plastidial thioredoxins: new functions and
759 new insights into specificity. *J Biol Chem* **278**: 23747–23752

760 **Collin V, Lamkemeyer P, Miginiac-Maslow M, Hirasawa M, Knaff DB, Dietz K-J,**
761 **Issakidis-Bourguet E** (2004) Characterization of plastidial thioredoxins from
762 Arabidopsis belonging to the new γ -type. *Plant Physiol* **136**: 4088–4095

763 **Cornic G, Bukhov NG, Wiese C, Bligny R, Heber U** (2000) Flexible coupling between
764 light-dependent electron and vectorial proton transport in illuminated leaves of C3
765 plants. Role of photosystem I-dependent proton pumping. *Planta* **210**: 468–477

766 **Courteille A, Vesa S, Sanz-Barrio R, Cazale A-C, Becuwe-Linka N, Farran I, Havaux**
767 **M, Rey P, Rumeau D** (2013) Thioredoxin m4 controls photosynthetic alternative
768 electron pathways in Arabidopsis. *Plant Physiol* **161**: 508–520

769 **Crozet P, Margalha L, Confraria A, Rodrigues A, Martinho C, Adamo M, Elias CA,**
770 **Baena-González E** (2014) Mechanisms of regulation of SNF1/AMPK/SnRK1 protein
771 kinases. *Front Plant Sci.* doi: 10.3389/fpls.2014.00190

772 **Da Q, Sun T, Wang M, Jin H, Li M, Feng D, Wang J, Wang H-B, Liu B** (2017) M-type
773 thioredoxins are involved in the xanthophyll cycle and proton motive force to alter NPQ
774 under low-light conditions in Arabidopsis. *Plant Cell Rep* **37**: 279–291

775 **Dreyer A, Dietz K-J** (2018) Reactive oxygen species and the redox-regulatory network in
776 cold stress acclimation. *Antioxidants* **7**: 169

777 **Dreze M, Monachello D, Lurin C, Cusick ME, Hill DE, Vidal M, Braun P** (2010) High-

778 quality binary interactome mapping. *Methods Enzymol.* doi: 10.1016/S0076-
779 6879(10)70012-4

780 **Emanuelsson O, Nielsen H, Brunak S, von Heijne G** (2000) Predicting subcellular
781 localization of proteins based on their N-terminal amino acid sequence. *J Mol Biol* **300**:
782 1005–1016

783 **Ereño-Orbea J, Oyenarte I, Martínez-Cruz LA** (2013) CBS domains: Ligand binding sites
784 and conformational variability. *Arch Biochem Biophys.* doi: 10.1016/j.abb.2013.10.008

785 **Fang L, Hou X, Lee LYC, Liu L, Yan X, Yu H** (2011) AtPV42a and AtPV42b redundantly
786 regulate reproductive development in *Arabidopsis thaliana*. *PLoS One* **6**: 21–23

787 **Fisher N, Bricker TM, Kramer DM** (2019) Regulation of photosynthetic cyclic electron
788 flow pathways by adenylate status in higher plant chloroplasts. *Biochim Biophys Acta -*
789 *Bioenerg* **1860**: 148081

790 **Geigenberger P, Thormählen I, Daloso DM, Fernie AR** (2017) The unprecedented
791 versatility of the plant thioredoxin system. *Trends Plant Sci* **22**: 249–262

792 **Gelhaye E, Rouhier N, Navrot N, Jacquot JP** (2005) The plant thioredoxin system. *Cell*
793 *Mol Life Sci* **62**: 24–35

794 **Guillaumot D, Lopez-Obando M, Baudry K, Avon A, Rigail G, Falcon de Longevialle**
795 **A, Broche B, Takenaka M, Berthomé R, De Jaeger G, et al** (2017) Two interacting
796 PPR proteins are major *Arabidopsis* editing factors in plastid and mitochondria. *Proc*
797 *Natl Acad Sci* **114**: 201705780

798 **Hardie DG, Hawley S a.** (2001) AMP-activated protein kinase: The energy charge
799 hypothesis revisited. *BioEssays* **23**: 1112–1119

800 **Hertle AP, Blunder T, Wunder T, Pesaresi P, Pribil M, Armbruster U, Leister D** (2013)
801 PGRL1 is the elusive ferredoxin-plastoquinone reductase in photosynthetic cyclic
802 electron flow. *Mol Cell* **49**: 511–523

803 **Ignoul S, Eggermont J** (2005) CBS domains: structure, function, and pathology in human
804 proteins. *Am J Physiol Physiol* **289**: C1369–C1378

805 **Issakidis E, Saarinen M, Decottignies P, Jacquot J, Crétin C, Gadal P, Miginiac-Maslow**
806 **M** (1994) Identification and characterization of second regulatory disulfide bridge of
807 recombinant *Sorghum* leaf NADP-Malate Dehydrogenase. *J. Biol. Chem.* 269:

808 **James P, Halladay J, Craig EA** (1996) Genomic libraries and a host strain designed for
809 highly efficient two-hybrid selection in yeast. *Genetics* **144**: 1425–36

810 **Jeong B-C, Park SH, Yoo KS, Shin JS, Song HK** (2013a) Change in single cystathionine β -
811 synthase domain-containing protein from a bent to flat conformation upon adenosine

812 monophosphate binding. *J Struct Biol* **183**: 40–46

813 **Jeong B-C, Park SH, Yoo KS, Shin JS, Song HK** (2013b) Crystal structure of the single
814 cystathionine β -synthase domain-containing protein CBSX1 from *Arabidopsis thaliana*.
815 *Biochem Biophys Res Commun* **430**: 265–271

816 **Jones DT, Taylor WR, Thornton JM** (1992) The rapid generation of mutation data matrices
817 from protein sequences. *Comput Appl Biosci* **8**: 275–82

818 **Junesch U, Gräber P** (1987) The activation of the reduced chloroplast ATP-synthase by
819 Δ pH. *Prog. Photosynth. Res.* Springer Netherlands, Dordrecht, pp 173–176

820 **Jung KW, Kim YY, Yoo KS, Ok SH, Cui MH, Jeong BC, Yoo SD, Jeung JU, Shin JS**
821 (2013) A cystathionine- β -synthase domain-containing protein, CBSX2, regulates
822 endothelial secondary cell wall thickening in anther development. *Plant Cell Physiol.*
823 doi: 10.1093/pcp/pcs166

824 **Kemp BE** (2004) Bateman domains and adenosine derivatives form a binding contract. *J Clin*
825 *Invest* **113**: 182–184

826 **Kobayashi Y, Inoue Y, Furuya F, Shibata K, Heber U** (1979) Regulation of adenylate
827 levels in intact spinach chloroplasts. *Planta* **147**: 69–75

828 **Kumar S, Stecher G, Tamura K** (2016) MEGA7: Molecular evolutionary genetics analysis
829 Version 7.0 for bigger datasets. *Mol Biol Evol* **33**: 1870–1874

830 **Kushwaha HR, Singh AK, Sopory SK, Singla-Pareek SL, Pareek A** (2009) Genome wide
831 expression analysis of CBS domain containing proteins in *Arabidopsis thaliana* L. and
832 *Oryza sativa* L. reveals their developmental and stress regulation. *BMC Genomics* **10**:
833 200

834 **Lemaire SD, Michelet L, Zaffagnini M, Massot V, Issakidis-Bourguet E** (2007)
835 Thioredoxins in chloroplasts. *Curr Genet* **51**: 343–365

836 **Michelet L, Zaffagnini M, Marchand C, Collin V, Decottignies P, Tsan P, Lancelin J-M,**
837 **Trost P, Miginiac-Maslow M, Noctor G, et al** (2005) Glutathionylation of chloroplast
838 thioredoxin f is a redox signaling mechanism in plants. *Proc Natl Acad Sci* **102**: 16478–
839 16483

840 **Miyake C** (2020) Molecular mechanism of oxidation of P700 and suppression of ROS
841 production in Photosystem I in response to electron-sink limitations in C3 plants.
842 *Antioxidants* **9**: 230

843 **Monachello D, Guillaumot D, Lurin C** (2019) A pipeline for systematic yeast 2-hybrid
844 matricial screening in liquid culture. *Protoc Exch.* doi: 10.21203/rs.2.9948/v1

845 **Montrichard F, Alkhalfioui F, Yano H, Vensel WH, Hurkman WJ, Buchanan BB** (2009)

846 Thioredoxin targets in plants: The first 30 years. *J Proteomics* **72**: 452–474

847 **Murai R, Okegawa Y, Sato N, Motohashi K** (2021) Evaluation of CBSX proteins as
848 regulators of the chloroplast thioredoxin system. *Front Plant Sci.* doi:
849 10.3389/fpls.2021.530376

850 **Nakano H, Yamamoto H, Shikanai T** (2019) Contribution of NDH-dependent cyclic
851 electron transport around photosystem I to the generation of proton motive force in the
852 weak mutant allele of *pgr5*. *Biochim Biophys Acta - Bioenerg* **1860**: 369–374

853 **Nielsen H, Engelbrecht J, Brunak S, Heijne G Von** (1997) A neural network method for
854 identification of Prokaryotic and Eukaryotic signal peptides and prediction of their
855 cleavage sites. *Int J Neural Syst* **08**: 581–599

856 **Nikkanen L, Toivola J, Trotta A, Diaz MG, Tikkanen M, Aro E-M, Rintamäki E** (2018)
857 Regulation of cyclic electron flow by chloroplast NADPH-dependent thioredoxin
858 system. *Plant Direct* **2**: e00093

859 **Ok SH, Yoo KS, Shin JS** (2012) CBSXs are sensor relay proteins sensing adenosine-
860 containing ligands in *Arabidopsis*. *Plant Signal Behav* **7**: 664–7

861 **Okegawa Y, Motohashi K** (2015) Chloroplastic thioredoxin m functions as a major regulator
862 of Calvin cycle enzymes during photosynthesis *in vivo*. *Plant J* **84**: 900–913

863 **Okegawa Y, Motohashi K** (2020) M-type thioredoxins regulate the PGR5/PGRL1-
864 dependent pathway by forming a disulfide-linked complex with PGRL1. *Plant Cell* **32**:
865 3866–3883

866 **Pérez-Ruiz JM, Naranjo B, Ojeda V, Guinea M, Cejudo FJ** (2017) NTRC-dependent
867 redox balance of 2-Cys peroxiredoxins is needed for optimal function of the
868 photosynthetic apparatus. *Proc Natl Acad Sci U S A* **114**: 12069–12074

869 **Polge C, Thomas M** (2007) SNF1/AMPK/SnRK1 kinases, global regulators at the heart of
870 energy control? *Trends Plant Sci.* **12**: 20–28

871 **Pulido P, Spínola MC, Kirchsteiger K, Guinea M, Pascual MB, Sahrawy M, Sandalio**
872 **LM, Dietz KJ, González M, Cejudo FJ** (2010) Functional analysis of the pathways for
873 2-Cys peroxiredoxin reduction in *Arabidopsis thaliana* chloroplasts. *J Exp Bot* **61**: 4043–
874 4054

875 **Ramon M, Ruelens P, Li Y, Sheen J, Geuten K, Rolland F** (2013) The hybrid Four-CBS-
876 Domain KINby subunit functions as the canonical γ subunit of the plant energy sensor
877 SnRK1. *Plant J* **75**: 11–25

878 **Rey P, Sanz-Barrio R, Innocenti G, Ksas B, Courteille A, Rumeau D, Issakidis-Bourguet**
879 **E, Farran I** (2013) Overexpression of plastidial thioredoxins f and m differentially alters

880 photosynthetic activity and response to oxidative stress in tobacco plants. *Front Plant Sci*
881 **4**: 1–13

882 **Ruelland E, Lemaire-Chamley M, Le Maréchal P, Issakidis-Bourguet E, Djukic N,**
883 **Miginiac-Maslow M** (1997) An internal cysteine is involved in the thioredoxin-
884 dependent activation of sorghum leaf NADP-malate dehydrogenase. *J Biol Chem* **272**:
885 19851–19857

886 **Santarius KA, Heber U** (1965) Changes in the intracellular levels of ATP, ADP, AMP and
887 Pi and regulatory function of the adenylate system in leaf cells during photosynthesis.
888 *BBA - Biophys Incl Photosynth* **102**: 39–54

889 **Scholl RL, May ST, Ware DH** (2000) Seed and molecular resources for Arabidopsis. *Plant*
890 *Physiol* **124**: 1477–80

891 **Scott JW, Hawley S a., Green K a., Anis M, Stewart G, Scullion G a., Norman DG,**
892 **Hardie DG** (2004) CBS domains form energy-sensing modules whose binding of
893 adenosine ligands is disrupted by disease mutations. *J Clin Invest* **113**: 274–284

894 **Sekiguchi T, Yoshida K, Okegawa Y, Motohashi K, Wakabayashi K, Hisabori T** (2020)
895 Chloroplast ATP synthase is reduced by both f-type and m-type thioredoxins. *Biochim*
896 *Biophys Acta - Bioenerg* **1861**: 148261

897 **Shahbaaz M, Ahmad F, Imtaiyaz Hassan M** (2015) Structure-based functional annotation
898 of putative conserved proteins having lyase activity from *Haemophilus influenzae*. *3*
899 *Biotech* **5**: 317–336

900 **Shikanai T** (2016) Chloroplast NDH: A different enzyme with a structure similar to that of
901 respiratory NADH dehydrogenase. *Biochim Biophys Acta - Bioenerg* **1857**: 1015–1022

902 **Shin JS, So WM, Kim SY, Noh M, Hyoung S, Yoo KS, Shin JS** (2020) CBSX3-Trxo-2
903 regulates ROS generation of mitochondrial complex II (succinate dehydrogenase) in
904 Arabidopsis. *Plant Sci* **294**: 110458

905 **Stephan D, Slabber C, George G, Ninov V, Francis KP, Burger JT** (2011) Visualization
906 of plant viral suppressor silencing activity in intact leaf lamina by quantitative
907 fluorescent imaging. *Plant Methods*. doi: 10.1186/1746-4811-7-25

908 **Stitt M, Lilley RM, Heldt HW** (1982) Adenine nucleotide levels in the cytosol, chloroplasts,
909 and mitochondria of wheat leaf protoplasts. *Plant Physiol* **70**: 971–977

910 **Thormählen I, Meitzel T, Groysman J, Öchsner AB, von Roepenack-Lahaye E, Naranjo**
911 **B, Cejudo FJ, Geigenberger P** (2015) Thioredoxin f1 and NADPH-dependent
912 thioredoxin reductase C have overlapping functions in regulating photosynthetic
913 metabolism and plant growth in response to varying light conditions. *Plant Physiol* **169**:

914 pp.01122.2015

915 **Thormählen I, Zupok A, Rescher J, Leger J, Weissenberger S, Groysman J, Orwat A,**
916 **Chatel-Innocenti G, Issakidis-Bourguet E, Armbruster U, et al** (2017) Thioredoxins
917 play a crucial role in dynamic acclimation of photosynthesis in fluctuating light. *Mol*
918 *Plant* **10**: 168–182

919 **Usuda H** (1988) Adenine nucleotide levels, the redox state of the NADP system, and
920 assimilatory force in nonaqueously purified mesophyll chloroplasts from maize leaves
921 under different light intensities. *Plant Physiol* **88**: 1461–1468

922 **Vaseghi M-J, Chibani K, Telman W, Liebthal MF, Gerken M, Schnitzer H, Mueller SM,**
923 **Dietz K-J** (2018) The chloroplast 2-cysteine peroxiredoxin functions as thioredoxin
924 oxidase in redox regulation of chloroplast metabolism. *Elife* **7**: 1–28

925 **Voon CP, Guan X, Sun Y, Sahu A, Chan MN, Gardeström P, Wagner S, Fuchs P,**
926 **Nietzel T, Versaw WK, et al** (2018) ATP compartmentation in plastids and cytosol of
927 *Arabidopsis thaliana* revealed by fluorescent protein sensing. *Proc Natl Acad Sci*
928 201711497

929 **Waese J, Fan J, Pasha A, Yu H, Fucile G, Shi R, Cumming M, Kelley LA, Sternberg**
930 **MJ, Krishnakumar V, et al** (2017) ePlant: Visualizing and exploring multiple levels of
931 data for hypothesis generation in plant biology. *Plant Cell* **29**: 1806–1821

932 **Wang F, Yan J, Ahammed GJ, Wang X, Bu X, Xiang H, Li Y, Lu J, Liu Y, Qi H, et al**
933 (2020) PGR5/PGRL1 and NDH mediate far-red light-induced Photoprotection in
934 response to chilling stress in Tomato. *Front Plant Sci* **11**: 1–18

935 **Xiao B, Sanders MJ, Underwood E, Heath R, Mayer F V., Carmena D, Jing C, Walker**
936 **PA, Eccleston JF, Haire LF, et al** (2011) Structure of mammalian AMPK and its
937 regulation by ADP. *Nature* **472**: 230–233

938 **Yamori W, Sakata N, Suzuki Y, Shikanai T, Makino A** (2011) Cyclic electron flow around
939 photosystem I via chloroplast NAD(P)H dehydrogenase (NDH) complex performs a
940 significant physiological role during photosynthesis and plant growth at low temperature
941 in rice. *Plant J* **68**: 966–976

942 **Yamori W, Shikanai T** (2016) Physiological functions of cyclic electron transport around
943 Photosystem I in sustaining photosynthesis and plant growth. *Annu Rev Plant Biol* **67**:
944 81–106

945 **Yamori W, Shikanai T, Makino A** (2015) Photosystem I cyclic electron flow via chloroplast
946 NADH dehydrogenase-like complex performs a physiological role for photosynthesis at
947 low light. *Sci Rep* **5**: 13908

- 948 **Yoo KS, Ok SH, Jeong B-C, Jung KW, Cui MH, Hyung S, Lee M-R, Song HK, Shin JS**
949 (2011) Single cystathionine β -synthase domain-containing proteins modulate
950 development by regulating the thioredoxin system in Arabidopsis. *Plant Cell* **23**: 3577–
951 3594
- 952 **Yoshida K, Hara S, Hisabori T** (2015) Thioredoxin selectivity for thiol-based redox
953 regulation of target Proteins in Chloroplasts. *J Biol Chem* **290**: 14278–14288
- 954 **Yoshida K, Hisabori T** (2018) Determining the rate-limiting step for light-responsive redox
955 regulation in chloroplasts. *Antioxidants* **7**: 153
- 956

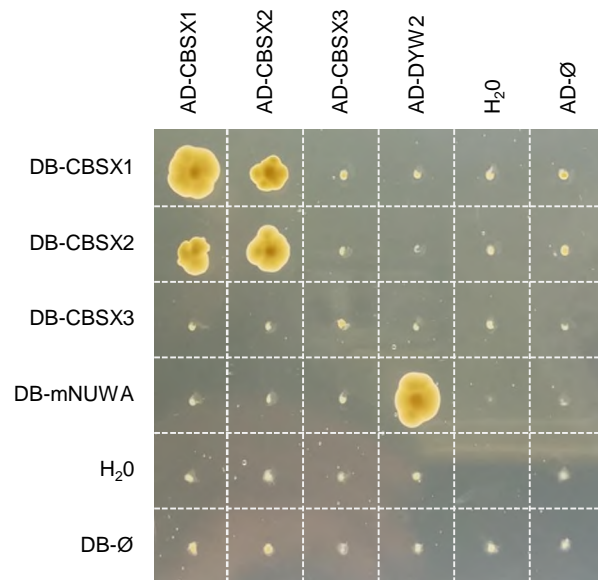


Figure 1. Protein interactions between Arabidopsis CBSX isoforms assayed by yeast 2-hybrid.

Interactions were tested using a mating-based Y2H matricial assay with AD fusions on the horizontal axis and the DB fusions on the vertical axis. In the “H₂O” row and column, yeast cells were replaced by water; in the “Ø” row and column, mating was performed with yeasts transformed with an empty vector. As a positive interaction control, we used DB-mNUWA and AD-mDYW2 (Guillaumot et al., 2017). Interactions were tested on selective medium without histidine.

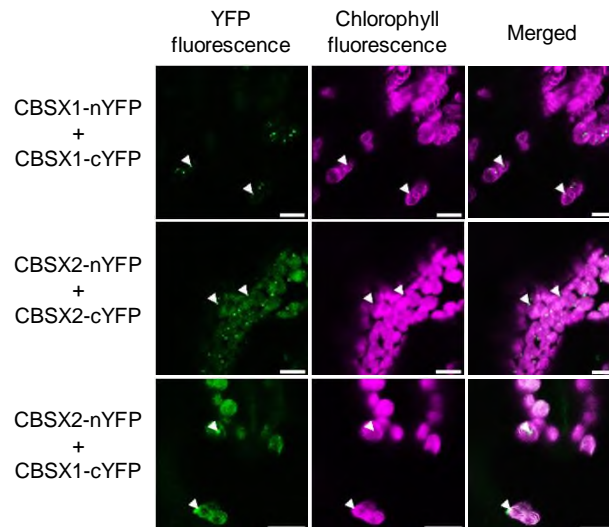


Figure 2. *In planta* protein interactions between CBSX isoforms assayed by BiFC.

BiFC of YFP in transiently transformed *Nicotiana benthamiana* leaves. Left column, YFP fluorescence signal. Middle column, chlorophyll fluorescence signal. Right column, merge of fluorescent signals. Fluorescence spots confirmed as YFP fluorescence signals by spectral analysis are indicated by white arrows. Observations were performed four days after transformations. Bars=10 μ m.

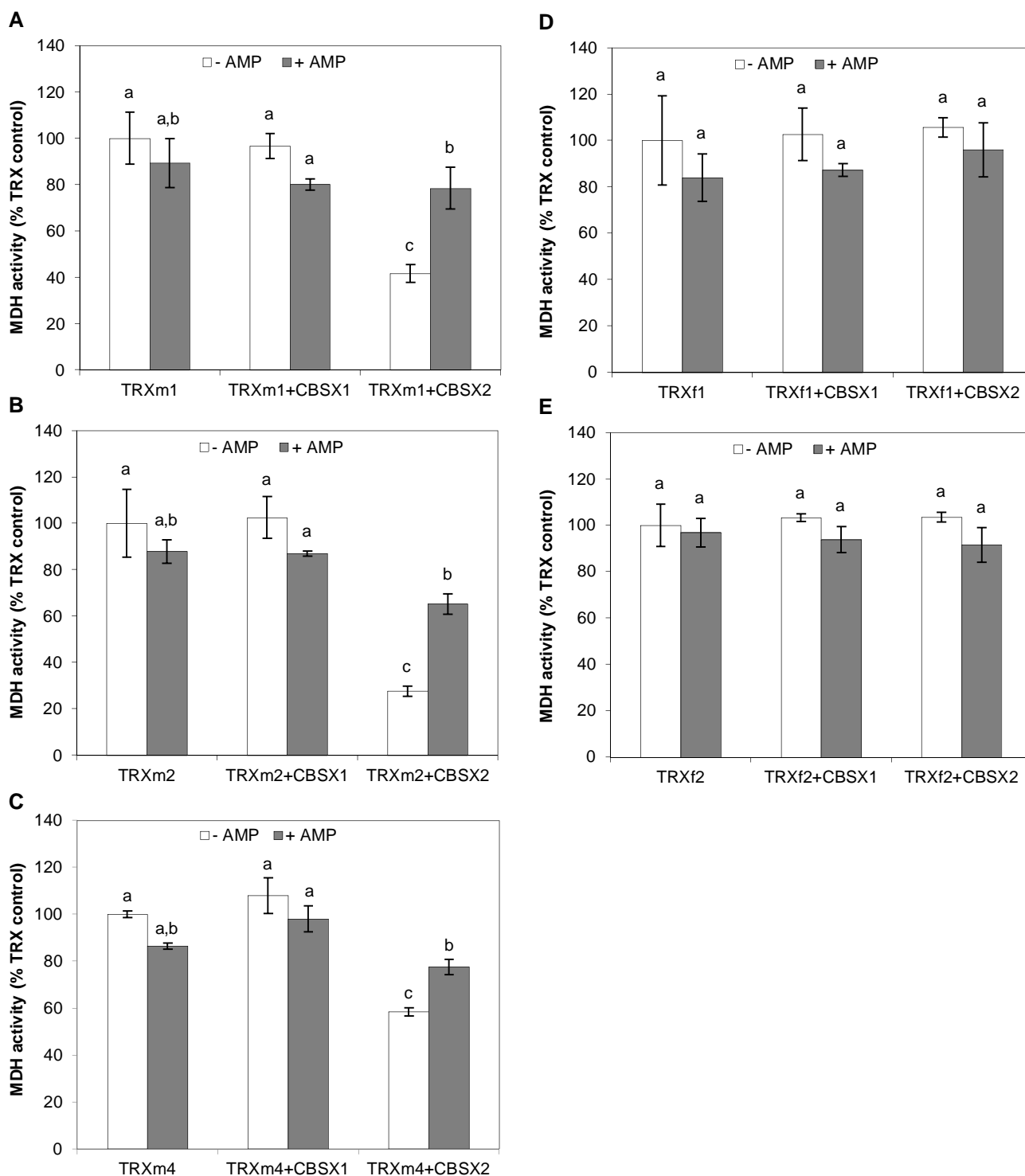


Figure 3. Effect of CBSX1 and 2 on TRX capacity to activate wild-type NADP-MDH, and effect of AMP.

NADP-MDH activation was measured after 20 min incubation at room temperature in presence of 10 μ M TRX (except TRXf1 at 1 μ M) and 10 mM DTE. 100% activation rate corresponds to the activation with DTE-reduced TRX (without CBSX and AMP). (A) TRXm1 (mean SA = 372 u/mg), (B) TRXm2 (mean SA = 314 u/mg), (C) TRXm4 (mean SA = 383 u/mg), (D) TRXf1 (mean SA = 432 u/mg) and (E) TRXf2 (mean SA = 340 u/mg). CBSX1/2 and AMP final concentration were 30 μ M and 1 mM, respectively. Values are means \pm SD (n=4). Bars with different letters correspond to significantly different values. P < 0.05. SA: specific activity of NADP-MDH at maximal activation (100%) expressed in units (u: μ mole NADPH oxidized per min) per mg of enzyme.

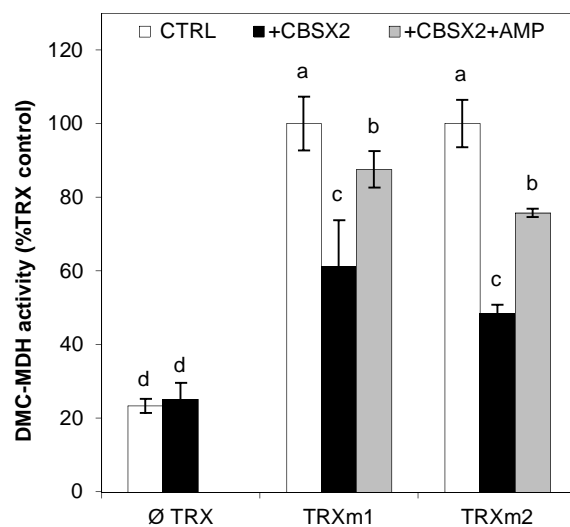


Figure 4. Effect of CBSX2 on mutant DMC-MDH activity and TRXm-dependent activation, and effect of AMP.

DMC-MDH activation was measured after 20 min incubation at room temperature in presence of DTE alone (Ø TRX) or DTE + TRXm1 or DTE + TRXm2. 100% activation rate corresponds to the maximal activation of DMC-MDH by DTE-reduced TRXm1/2 (without CBSX and AMP). Mean specific activity of DMC-MDH at maximal activation (100%) were 391 u/mg and 382 u/mg, with TRXm1 and TRXm2, respectively. Values are means \pm SD (n=4). TRXm1/2, CBSX2 and AMP were at a final concentration of 10 μ M, 30 μ M and 1 mM, respectively. Bars with different letters correspond to significantly different values. $P < 0.05$.

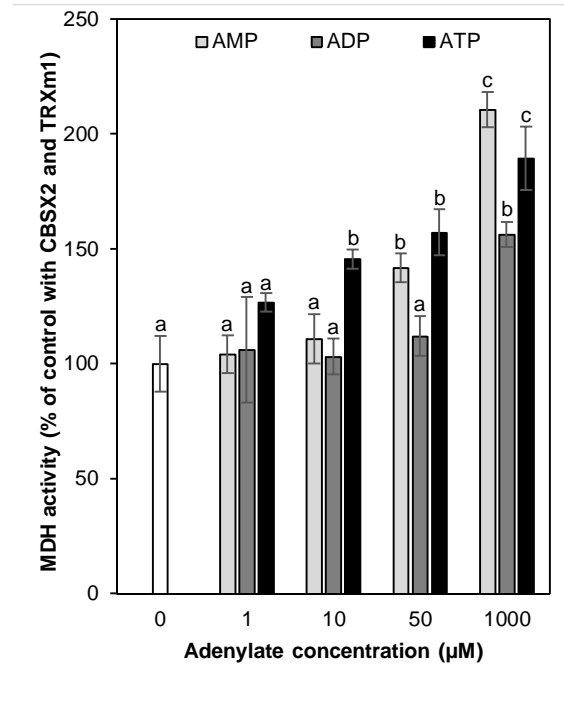


Figure 5. Effects of adenylates on CBSX2 inhibition of TRXm-dependent NADP-MDH activation.

Wild-type MDH activation was measured after 20 min incubation in presence of DTE-reduced TRXm1 (10 µM) with CBSX2 (30 µM) and 0, 1, 10, 50 or 1000 µM of AMP, ADP or ATP. Values are means ± SD (n=4-6). Bars with different letters correspond to significantly different values. $P < 0.05$.

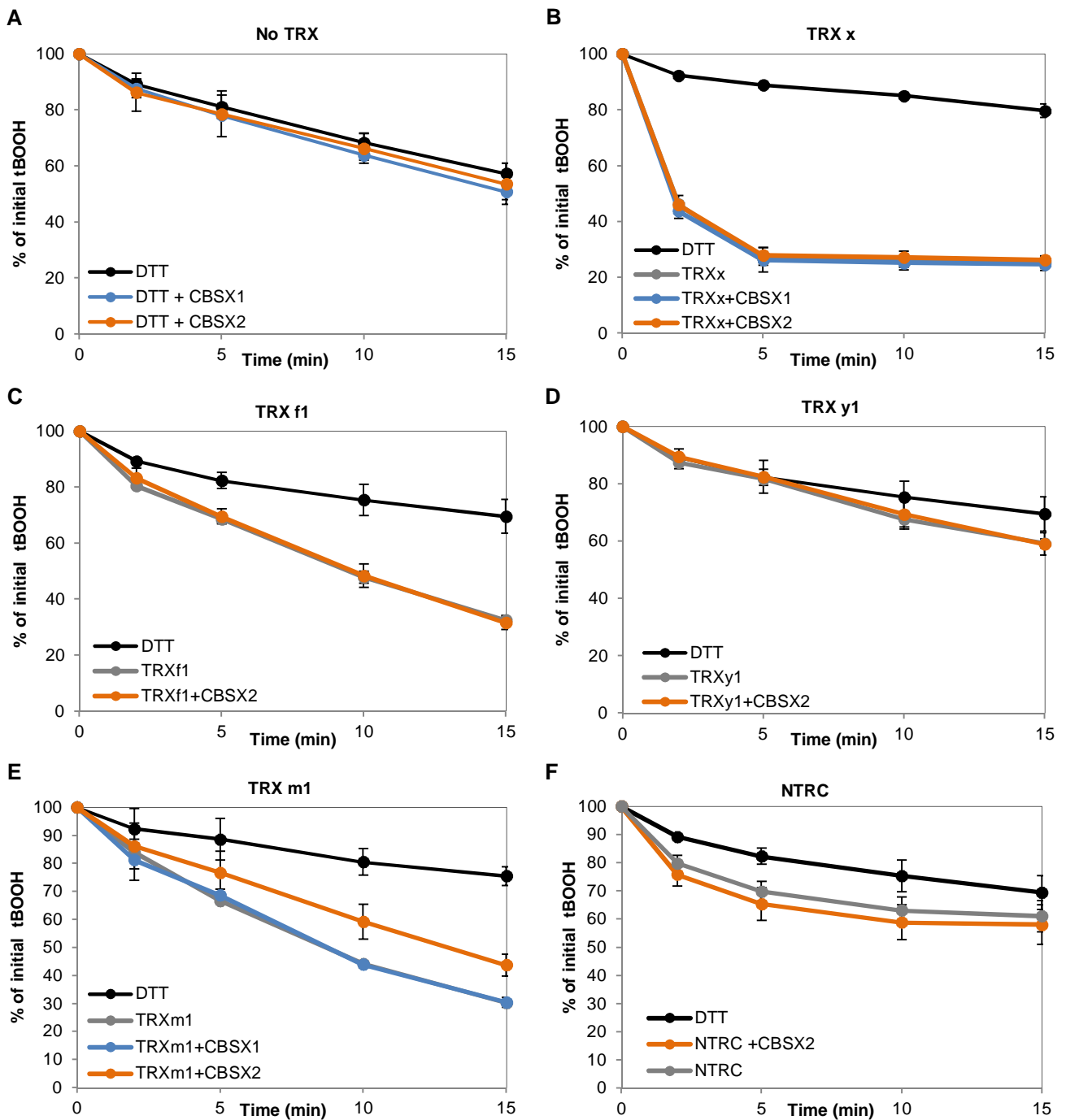


Figure 6. Effect of CBSX1 and 2 on 2-Cys PRX activity.

Time course of tBOOH reduction by 2-Cys PRXA was quantified by the FOX assay in presence of DTT alone (black curves), DTT-reduced TRX (grey curves), DTT-reduced TRX and CBSX1 (blue curves) or DTT-reduced TRX and CBSX2 (orange curves). (A) DTT alone; (B) DTT + TRX x; (C) DTT + TRX f1; (D) DTT + TRX y1; (E) DTT + TRX m1; (F) DTT + NTRC. The values are means \pm SD (n=3).

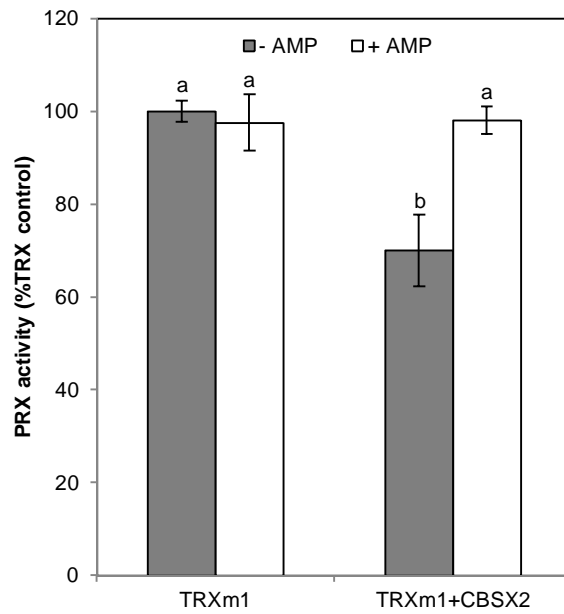


Figure 7. Effect of 1 mM AMP on CBSX2 towards TRXm1-dependent 2-Cys PRX activity.

2-Cys PRX activities were defined as the tBOOH reduction kinetic slope between 2 and 10 min and were normalized to the activity in the control condition (without CBSX and AMP) considered as 100%. The values are means \pm SD (n=3). Bars with different letters correspond to significantly different values. $P < 0.05$.

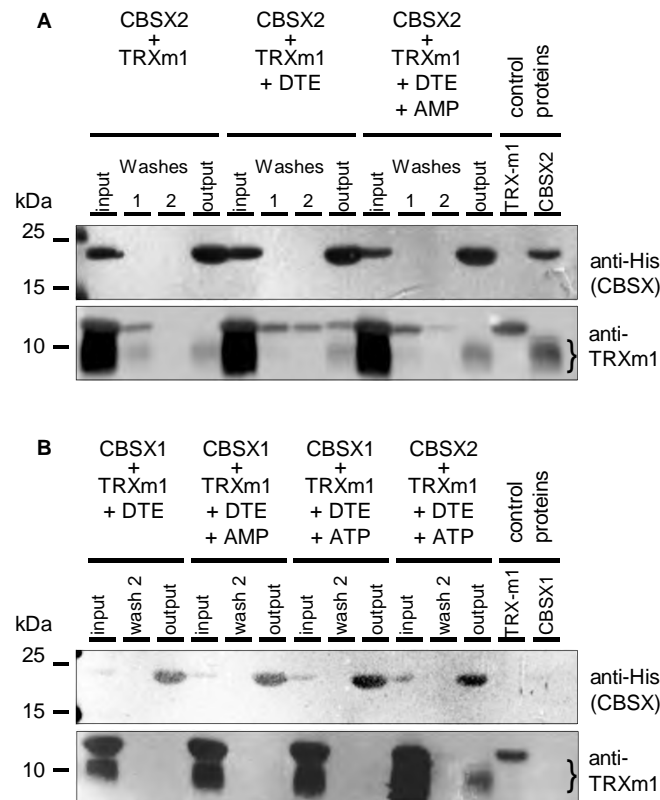


Figure 8. Pull-down assays with CBSX and TRXm proteins.

Pull-down of His-CBSX and TRXm1 in absence or presence of DTE, AMP and ATP. (A) Impact of 1 mM AMP and DTE on CBSX2-TRXm1 interaction. (B) Impact of 1 mM ATP or 1 mM AMP on CBSX-TRXm1 interaction. Input corresponds to proteins initially mixed before incubation with His-affinity agarose beads. Output corresponds to proteins eluted (after washes) from the resin by 200 mM imidazole. The bracket indicates an unspecific low molecular weight signal obtained using anti-TRXm1 antibodies on CBSX preparations.

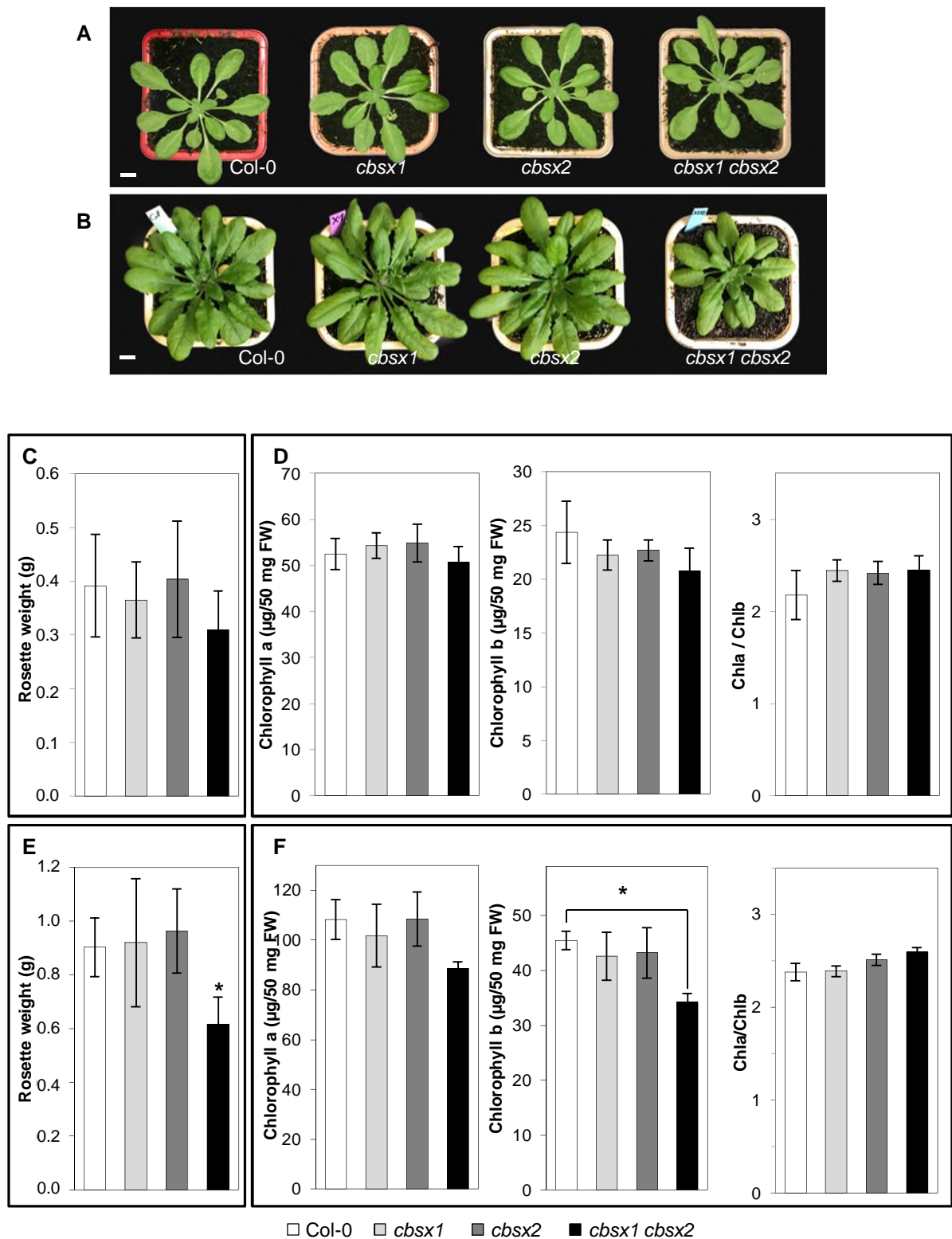


Figure 9. *cbsx* mutant phenotypes.

(A) Representative 5-week old plants grown in long day conditions at 20°C (bar = 1 cm). (B) Representative 11-week old plants grown in long day conditions at 12°C (bar = 1 cm). Plants images were digitally extracted for comparison. (C) and (D) Plants grown at control temperature. (E) and (F) Plants grown at low temperature. (C) and (E) Rosette fresh weight, values are means \pm SD (n=10), *: $P < 0.01$. (D) and (F) Chlorophyll (Chl) a and b contents, and Chla/Chlb ratios, values are means \pm SD (n=10). *: $P = 0.02$.

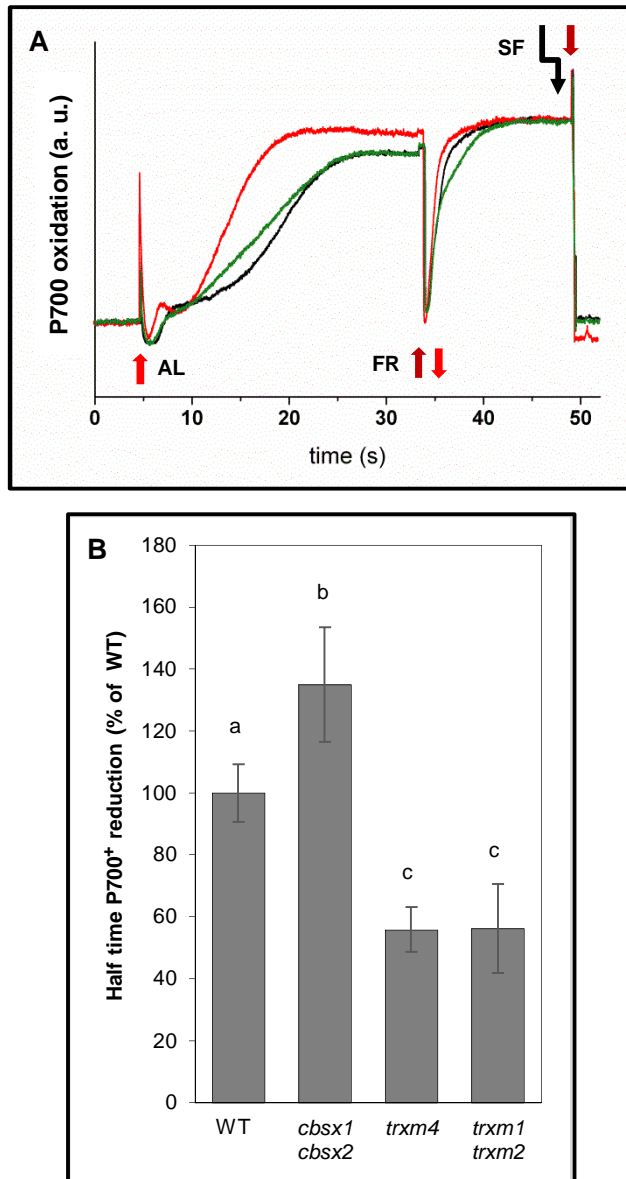


Figure 10. P700 measurements on leaves of wild-type plants and Trx m and CBSX-deficient mutants.

The redox state of the PSI primary donor P700 was monitored through the changes in absorbance at 830 versus 875 nm. (A) Representative curves are shown of plants kept at growth light intensity; WT: black, *cbsx1cbsx2*: red, *trxm1trxm2*: green. Leaves were illuminated with actinic red light, AL ($I = 830 \mu\text{mol photons}\cdot\text{m}^{-2}\cdot\text{s}^{-1}$) to oxidize P700 until a steady state was reached. Then far-red light, FR, was switched on. To achieve the maximum oxidation state a saturating flash, SF, was given at the end of the FR illumination. (B) Half-time of P700⁺ reduction after FR illumination of dark-adapted plants. The traces of the kinetics are shown in Figure S9. Values are means \pm SD ($n=4-6$). Bars with different letters correspond to significantly different values between genotypes. $P < 0.05$.

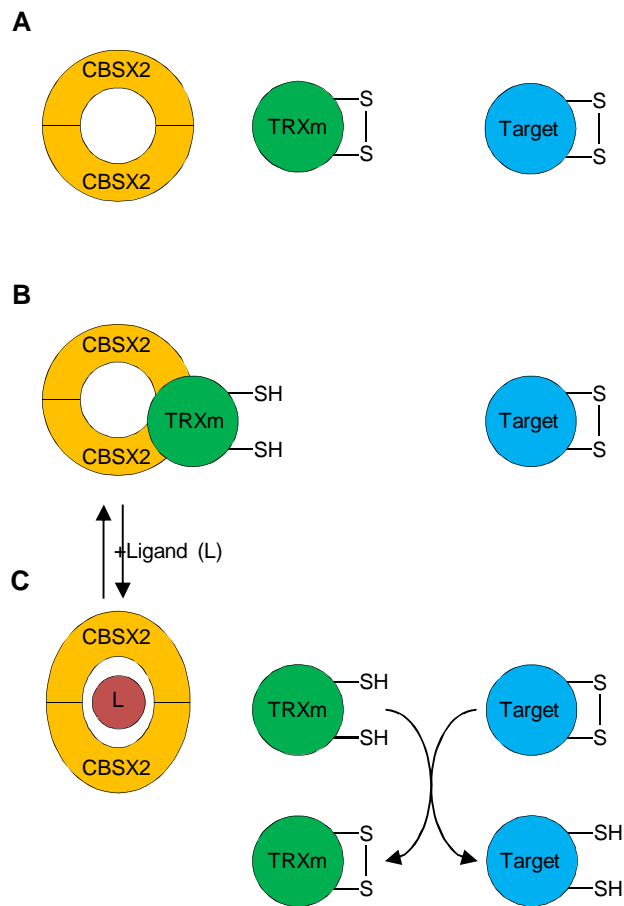
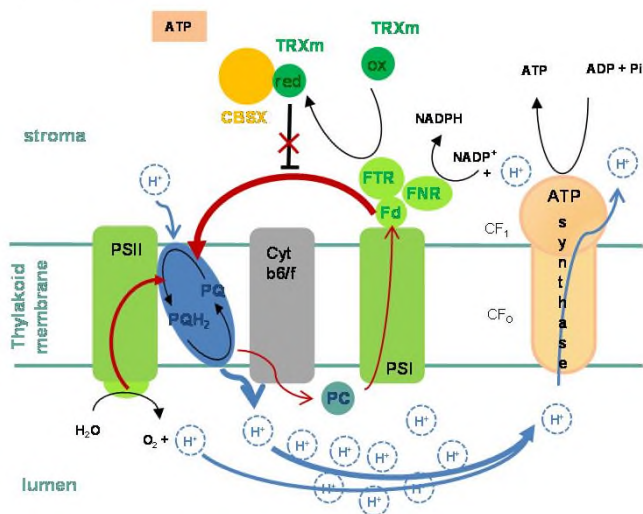


Figure 11. Model of TRX activity regulation by CBSX2.

CBSX2 homodimer (yellow disc) is unable to interact with oxidized TRX m (green circle) (A), but is able to interact with reduced TRXm and inhibits TRX m capacity to reduce its target (blue circle) (B). A conformational change of CBSX2 induced by adenosyl ligand (red circle) binding provokes the release of TRXm-CBSX2 interaction allowing TRXm to act on its target (C).

(A) Low ATP



(B) High ATP

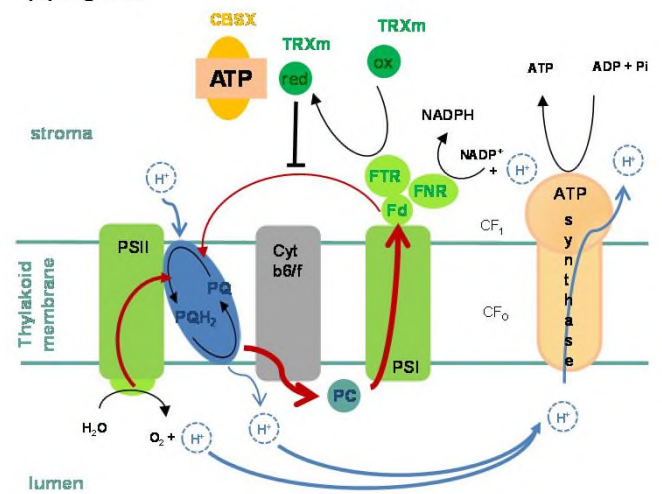


Figure 12. Model for functional relationship between CBSX and TRX in the context of ATP homeostasis in the chloroplast.

In the proposed model, when ATP level is low (A), CBSX can interact with TRX m, impeding its negative regulation of PSI-CET, which is primarily coupled to the generation of the proton motive force driving the synthesis of ATP by the thylakoid ATP synthase complex. When ATP level increases (B), ATP binds to CBSX, preventing interaction with TRX m and allowing down-regulation of the PSI-CET and thereby lowering ATP synthesis.

Electron and proton transfers are shown by red and blue arrows, respectively. Abbreviations are : PSII, photosystem I/II; Cyt b6/f, cytochrome b6/f complex; Fd, ferredoxin; FNR, ferredoxin-NADP reductase; FTR, ferredoxin/thioredoxin reductase; TRX, thioredoxin; CBSX, cystathionine- β -synthase domain protein; PQ, plastoquinone; PQH₂, plastoquinol; PC, plastocyanin; PSI-CET, cyclic electron transport around PSI ; CF₀ and CF₁, coupling factor 0 and 1 of chloroplast ATP synthase, respectively.

Supplemental data

Baudry et al., Plant Physiol 2022

Table S1. Primers used in the study.

Cloning:

CBSX1_start: GGAGATAGAACCATGGACGCCGTCCTTTACTC
CBSX1_intern: GGAGATAGAACCATGAGTGGAGTGACTACTGTTGG
CBSX1_end: TCCACCTCCGGATCCAGCATTCTATCACCAGAGC
CBSX1_stop: TCCACCTCCGGATCAAGCATTCTATCACCAGAGC
CBSX2_start: GGAGATAGAACCATGGGTTCAATCTCTTTATCC
CBSX2_intern: GGAGATAGAACCATGGCAAAAATGGAGGTTACACAG
CBSX2_end: TCCACCTCCGGATCCTGTAGAGTTCTCGGTTTCCC
CBSX2_stop: TCCACCTCCGGATCATGTAGAGTTCTCGGTTTCCC
CBSX3_start: GGAGATAGAACCATGCAAGGTGTGATTCGATCC
CBSX3_intern: GGAGATAGAACCATGAAAGGCTCTGTGCTGCAACA
CBSX3_end: TCCACCTCCGGATCCGTAACCTCCCTGAATATACGC
CBSX3_stop: TCCACCTCCGGATCAGTAACCTCCCTGAATATACGC

Genotyping:

SALK_LBa1: TGGTTCACGTAGTGGGCCATCG
Gabi_o8474: ATAATAACGCTGCGGACATCTACATTTT
cbsx1_LP: CGGGATTCGATCTTAGCCTAG
cbsx1_RP: TTATTGTGCATGGTAATTGCC
cbsx2_LP: TTTCCAGTACATTGCGTCATG
cbsx2_RP: CAGAAGTTCCAACGCTGAAAG

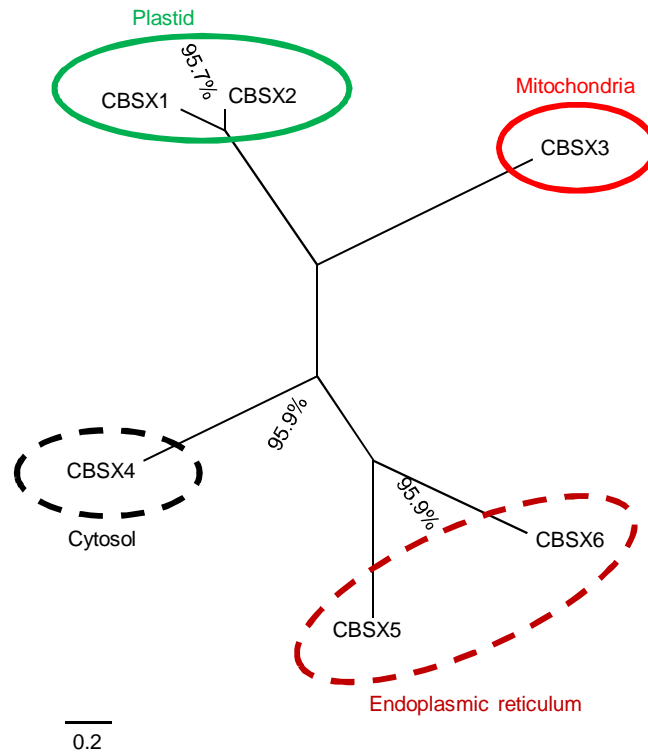


Figure S1. *Arabidopsis thaliana* CBSX phylogenetic tree.

Phylogenetic tree of the 6 *A. thaliana* CBSX, obtained by Maximum Likelihood algorithm and the Jones-Taylor-Thornton (JTT) model, bootstrap: 1000 using MEGA7.0.2. The scale bar represents 0.2 substitutions per position. Dashed lines indicate the predicted location according to Ok et al (2012). Continued lines indicate experimental location according to Yoo et al (2011), Jung et al (2013) and this work.

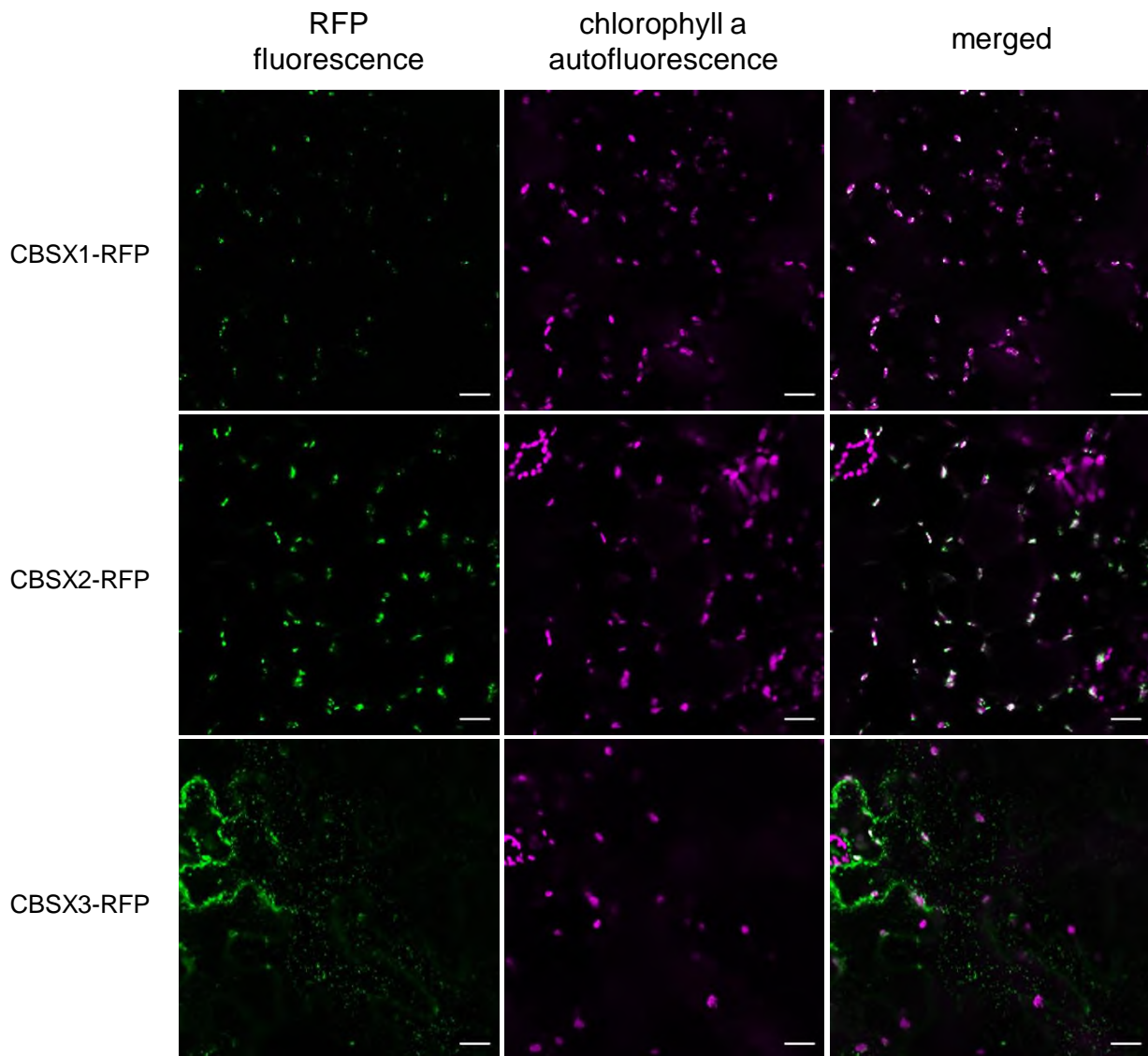


Figure S2. Subcellular localization of CBSX1, CBSX2 and CBSX3.

RFP signal from transiently transformed *Nicotiana benthamiana* leaves. All proteins were expressed as C-terminal fusions with RFP. Bars = 20 μ m.

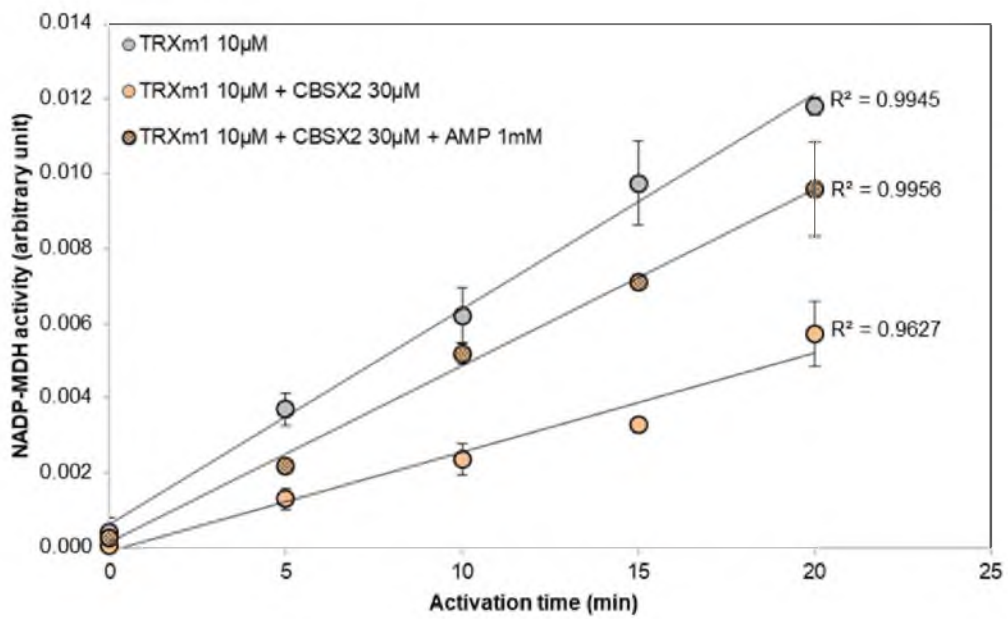


Figure S3. NADP-MDH activation kinetics.

Time course activation of wild-type NADP-MDH by DTE-reduced TRXm1 alone, with CBSX2, or with CBSX2 and AMP. The values are means \pm SD (n=3).

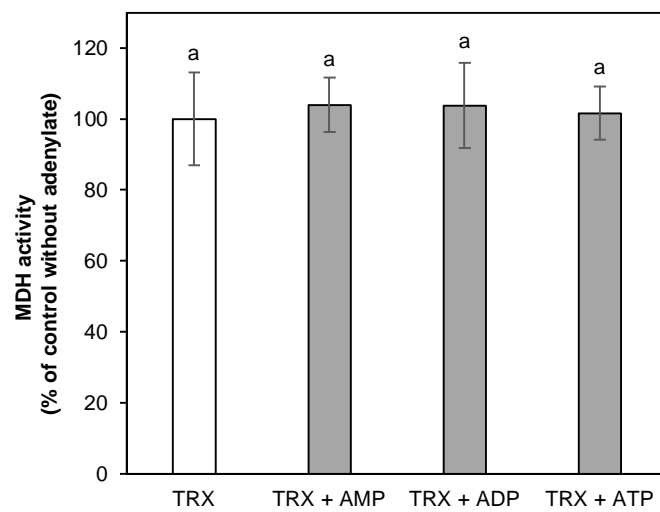


Figure S4. Test of direct effect of adenylylates on TRXm1-dependent NADP-MDH activation.

MDH activation by DTE-reduced TRXm1 without or with 1 mM AMP, ADP or ATP. The values are means \pm SD (n=3). $P < 0.05$

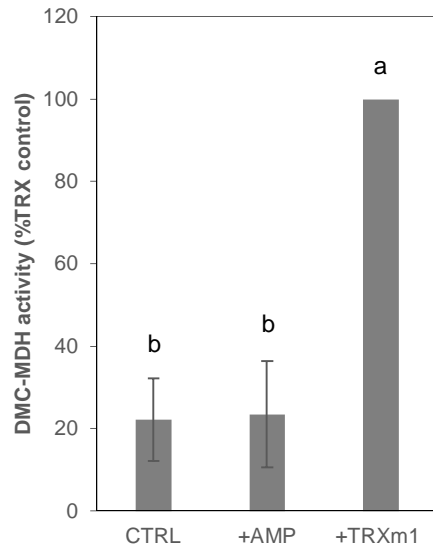


Figure S5. Effect of AMP on mutant DMC-MDH activity.

DMC-MDH activation was measured after 20 min incubation at room temperature in presence of DTE alone, with DTE and 1 mM AMP or with DTE and 30 μ M TRXm1. 100% activation rate corresponds to the maximal activation of DMC-MDH by DTE-reduced TRXm1. Values are means \pm SD (n=5). Bars with different letters correspond to significantly different values. $P < 0.05$.

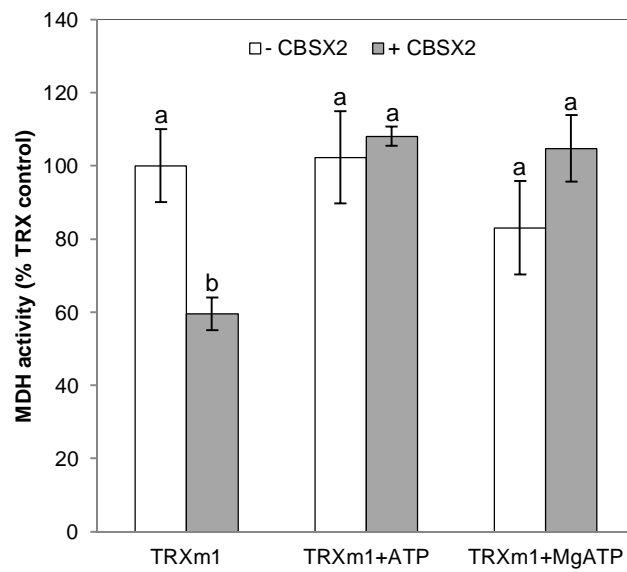


Figure S6. Effect of ATP on CBSX2 towards TRXm1-dependent NADP-MDH activation.

MDH activation by DTE-reduced TRX m1 in absence or in presence of CBSX2 and 1 mM ATP or MgATP. The values are means \pm SD (n=3). Bars with different letters correspond to significantly different values. $P < 0.05$.

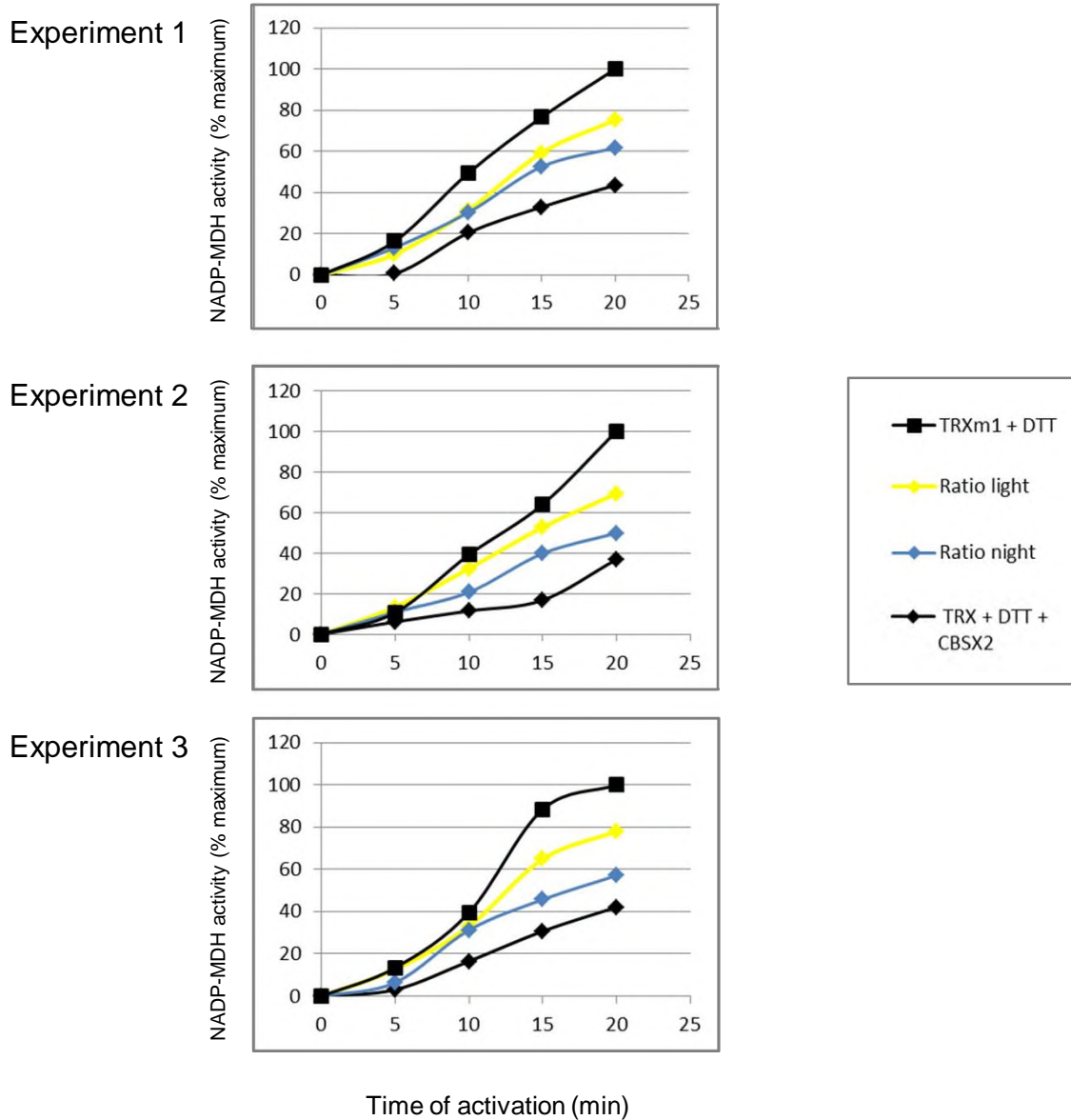


Figure S7. Effects of ATP together with ADP at concentrations and ratios mimicking light and night conditions on CBSX2 towards TRXm1-dependent NADP-MDH activation.

Time course of NADP-MDH activation by DTT-reduced TRX m1 in presence of CBSX2 without, and with adenylates at an ATP/ADP ratio of 2.5 (corresponding to light condition, yellow curve) or 0.3 (corresponding to night condition, blue curve). Adenylates total concentration was 2.0 and 1.3 mM in light and night mimicking conditions, respectively. Data from 3 independent experiments are shown.

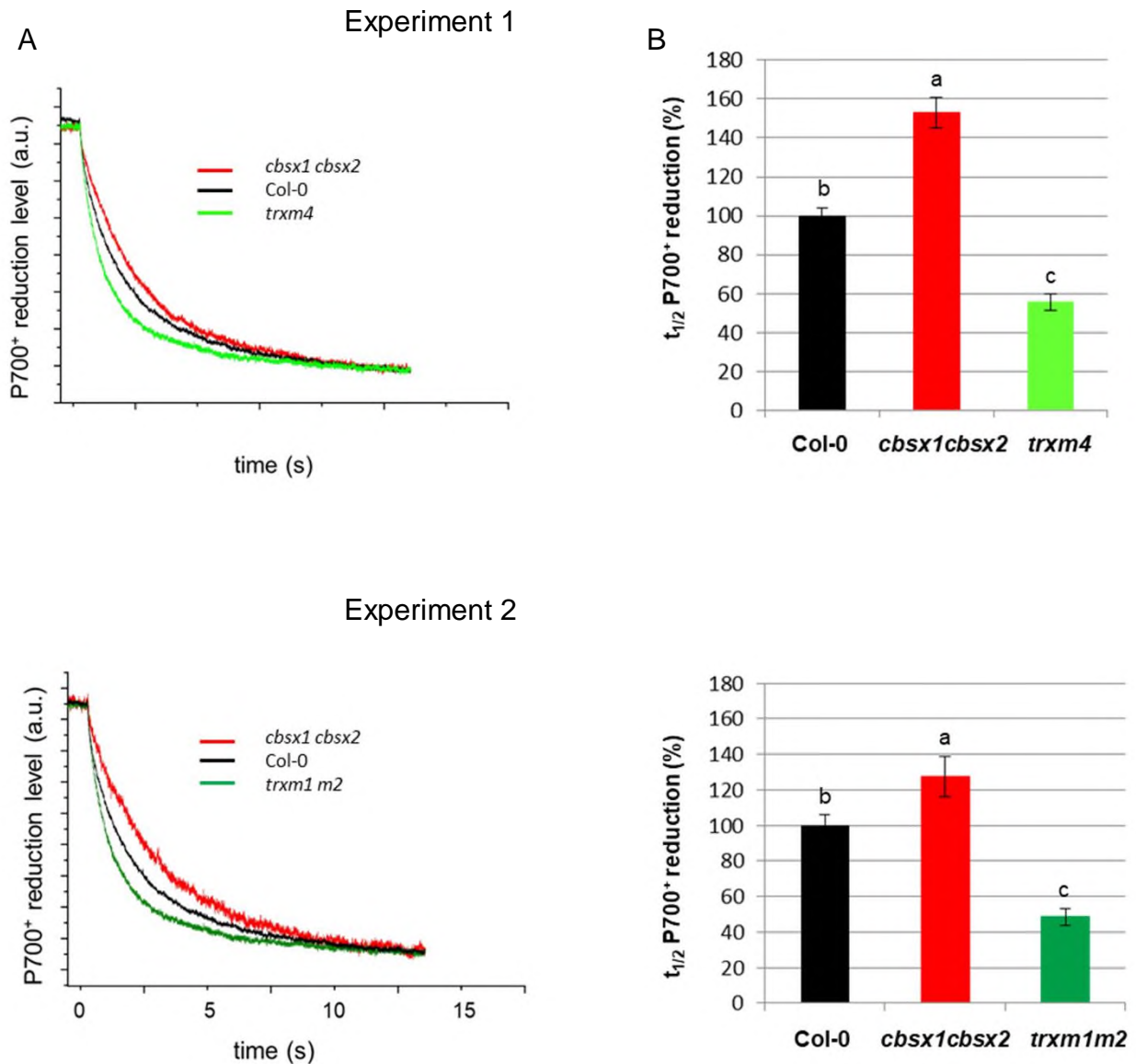


Figure S8. P700⁺ reduction.

P700⁺ reduction was monitored after 1 min FR illumination of dark-adapted plants of Col-0, TRX m single and double mutants, and in *cbsx1 cbsx2*. (A) Representative curves for the different genotypes. (B) Differences in the half-times of P700⁺ reduction normalized to Col-0. Values (in sec) were: 1.21 ± 0.10 , 1.84 ± 0.24 , 0.67 ± 0.09 for Col-0, *cbsx1cbsx2* and *trxm4*, respectively in experiment 1; and 0.83 ± 0.10 , 1.05 ± 0.13 , 0.40 ± 0.08 for Col-0, *cbsx1cbsx2* and *trxm1m2*, respectively in experiment 2. The values are means \pm SD (n=3-4). Bars with different letters correspond to significantly different values. $P < 0.01$.

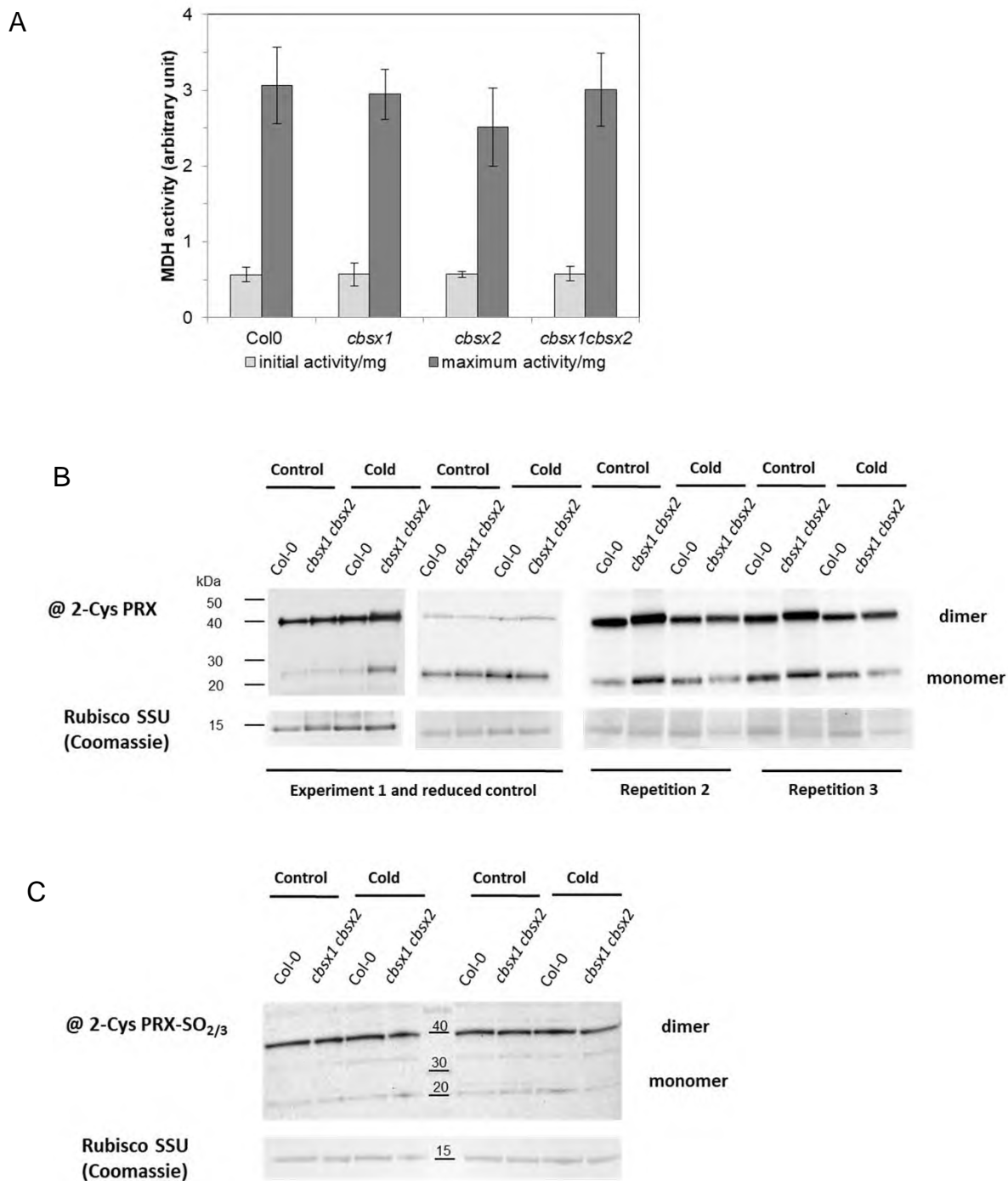


Figure S9. TRX targets in the context of CBSX mutations.

- (A) NADP-MDH leaf extractable activity in Col-0, CBSX1/2 single and double Arabidopsis mutant plants grown in control conditions. Activities were measured without (initial activity of the enzyme) or after pretreatment (reductive activation giving the maximal activity *i.e.* the enzyme capacity) of extracts with 10 mM DTE and 10 μ M TRX m1 20 min at room temperature. The values are means \pm SD (n=3).
- (B) 2-Cys PRX oligomeric state in Col-0, and CBSX1/2 single and double Arabidopsis mutant plants grown in control or cold conditions. Total leaf protein extracts (50 μ g) were electrophoresed in non-reducing conditions and transferred onto a PVDF membrane for 2-Cys PRX immuno-detection. Reduction treatment (DTT 50 mM 30 min at RT prior SDS-PAGE) was performed as control to validate dimer and monomer corresponding to the oxidized and reduced form, respectively.
- (C) Detection of over-oxidized 2-Cys PRX (2-Cys PRX-SO_{2/3}).